Processing double refractory gold-arsenic-bearing concentrates by direct reductive melting

Ainur Seitkan, Simon Redfern

July 22, 2016

Abstract

Iron arsenides may be the key to extraction of gold from existing refractory ores such as that at Bakyrchik, Kazakhstan, an ore body containing an estimated £8.5 billion reserve of gold. Gold is not extractable without significant ecological contamination from the associate arsenopyrite mineralisation. A new method for gold recovery from refractory gold-arsenic-bearing materials, based on direct reductive melting (DRM) of the concentrate has been developed, which locks As into relatively benign iron arsenide phases, while gold is extracted into lead alloy. The method has been filed as a patent with the Patent Office of the Republic of Kazakhstan.

Keywords

Bakyrchik; Double refractory gold-arsenic-bearing concentrate; Direct reductive melting; Thermodynamic modelling; Process optimisation

1 Introduction

Mining metallurgists classify gold ores into two categories according to their amenability to a conventional "cyanidation-carbon adsorption" gold extraction technology: "free milling" and "refractory" [1]. The former are those ores from which more than 90% of the gold can be extracted by simple gravity techniques or direct conventional cyanide leaching, whilst under the same treatment the latter ores give much lower recovery and require more complex methods to release gold [2]. The term double refractory is applied when refractoriness of the gold ore is exacerbated by the presence of preg-robbing carbonaceous material. The problem of double refractory ores is not well understood. It is a current topic of investigation by a few mining companies and research groups in terms of processing. Several pre-cyanidation treatment methods have been developed for double refractory gold ores, such as flotation and depression, blanking, the use of activated carbon or resin in the leach, roasting, chemical oxidation and bioleaching. These technologies are reviewed in details by Afenya [3]. However, in most cases they do not guarantee high gold recovery upon cyanidation [4,5]. Double refractory ores are found across the globe [6–13]. For example, Nevada, Mother Lode, Gold Quarry, Gold Acres,

Getchell Mine, Maggie Creek, and Jerritt Canyon in the United States of America; McIntrye Porcupine, Kerr Anderson, and Gold Strike in Canada; Prestea, Ashanti, and Bogosu Mine in Ghana; Natalkinck in Russia; Witwatersrand in South Africa; Bakyrchik in Kazakhstan, Morro Velho and Queiroz Mine in Brazil, Cosmo Howley and Fortnum in Australia; Waihi/Paeroa in New Zealand; Laizhou and Neilanggou in China.

Of all nations, the Republic of Kazakhstan has the sixth largest reserves of gold [14]. With the depletion of the oxide lode deposits, gold extraction is moving towards the mining of increasingly technologically difficult ores in Kazakhstan and generally throughout the world [2]. We have focussed on Bakyrchik ore as an accessible example of a generic type of refractory ore that is now being considered for exploitation across the globe. The Bakyrchik ore deposit is the largest native gold deposit in Kazakhstan and one of the largest gold deposits in the world. It is a part of Kyzyl Gold Project, which also includes Bolshevik gold deposit (Figure 1). According to a feasibility study carried out by the international mining consultants Roscoe Postle Associates, based on drill hole data available on 31 July 2013, the Bakyrchik deposit contains approximately 10.5 Moz of gold (300 t) [15], with an equivalent value of more than £8.5 billion. The deposit is located in the Auezov village in north-eastern Kazakhstan, about 75 km south-west of East Kazakhstan's centre, the city Oskemen (previously known as Ust-Kamenogorsk), which is built on the non-ferrous metals industry. The mine has road and railway connections to Europe, Russia, and China.

Figure 1: Kyzyl Gold Project [16].

Bakyrchik is a hydrothermal gold-ore deposit within the Kalba gold belt [17]. It consists of a series of mineralized lenses lying within the 11.5 km long Kyzyl Shear Zone, defined in the early 1950s by surface trenching. Gold mineralization is hosted within sheared carbonaceous sediments in the fault zones, and is principally contained within sulfide mineralization. The geology and mineralization of Bakyrchik has been previously described [18]. The mineralogical composition of the ore is represented by three main mineral associations [17]: (1) pyrrhotite, globular pyrite, marcasite, gregite, pyrite, and carbonates (the so-called "barren stage"); (2) quartz, pyrite, arsenopyrite, and gold (known as the "first productive stage"); (3) pyrite, sphalerite, galena, chalcopyrite, tennantite and tetrahedrite, bismuthinite, and aikinite (the "second productive stage"). The total sulfide content of the ore varies from 0.5 to 10%. Throughout, gold is dispersed

in pyrite and arsenopyrite in the form of microscopic and submicroscopic inclusions. Larger gold particles (up to 1 mm in size) are found along microfractures in pyrite and arsenopyrite, and occur in association with galena, sphalerite, chalcopyrite, quartz, and carbonate. Gold can also be found as inclusions in quartz-sericite-carbonate assemblages, surrounding sulfides. Free gold of 900 fineness (90% in the alloy) constitutes no more than 10% of the recovered amount and has a positive correlation with arsenic. The quartz in shear zones does not contain gold [19].

Refractoriness of Bakyrchik ore. Mineralogical studies indicate that the majority of the gold is encapsulated by arsenopyrite and, to a lesser extent, pyrite (Table 1). Cyanides are unable to access the locked gold. Hence it is necessary to induce decomposition of iron sulfide minerals in order to release the gold particles. All pre-treatment processes are based on the oxidative destruction of sulfides: thermal, chemical or biological [20].

Table 1: Gold and other admixture elemental concentrations in the monomineralic fractions of pyrite and arsenopyrite of the Bakyrchik ore, ppm [17]

Mineral	Pb	Cu	Zn	Ni	Co	Ga	Sb	As	Ag	Au
Pyrite	1100	300	2500	1500	950	-	1000	60000	-	25
Arsenopyrite	50	400	1300	300	250	2	300	60000	8	400

The refractoriness of the Bakyrchik ore is also exacerbated by the presence of carbonaceous matter (up to 4%), which has high sorption capacity with respect to gold-cyanide complexes or pregnant leach solution, and further excludes the use of conventional cyanide leaching methods. Carbon removal at the enrichment step usually significantly reduces subsequent gold recovery. Direct cyanide leaching of the Bakyrchik concentrates allows recovery of only 26-28% of the gold.

Further difficulties arise from the presence of arsenic in the ore - up to 1.4%. This complicates recovery because, although roasting can potentially liberate gold, in air this would be accompanied by arsenic release into the atmosphere in the form of As_2O_3. The significant quantity of arsenic in the concentrate during roasting raises serious environmental concerns. The condensation of As_2O_3 remains the principal problem in roasting, in terms of its hazardous nature in both air and water contamination. Furthermore, safe disposal of the arsenic compounds in the mine waste, in adherence with environmental legislative norms, is problematic.

Brief history of gold mining. Bakyrchik gold mine commenced production with open pit mining (1956-1994) to provide gold-bearing flux to copper smelters in Ust-Kamenogorsk (Oskemen). Subsequently, underground mining occurred between 1963 and 1997. Overall 3.8 Mt ore has been mined at 7.3 g/t grade. When Kazakhstan became independent in 1992 Minproc Holdings of Australia, Chilewich International of New York and the Kazakhstan government formed an international joint venture to operate Bakyrchik. A pilot-scale processing plant with a capacity of 150 000 t/yr was constructed in 1994, incorporating comminution, conventional flotation, nitric-acid sulfide oxidation (so called Redox-processing) and Carbon-in-Pulp (CIP) methods. The compositions of the test-batches of concentrates varied over a wide range of values (%): 6-14 As, 15-28 Fe, 16-28 S, 6-12 C, 6-12 CaO and MgO, 60-90 g/t of Au, and 15-22 g/t of Ag. However, the joint venture option was abandoned following disapointing results.

In 1996 Ivanhoe Mines Ltd acquired an interest in the Bakyrchik deposit. Various commercial metallurgical alternatives to processing the refractory ores had been tested at Bakyrchik, such as BIOX (biooxi-

dation), single stage oxidative roasting, and two-stage oxidative roasting. Eventually, it was concluded that circulating fluid-bed roasting would provide optimum recoveries. A 100000 kt/yr pilot plant was constructed to evaluate the viability of single-stage roasting, using a rotary kiln. The pilot roaster operated at Bakyrchik only in late 2009. The operation was ceased in 2010 due to disappointingly low gold recovery rates (between 30% and 60%)[21].

In January 2012 the Rio Tinto Group obtained control of Turquoise Hill Resources Ltd. (formerly Ivanhoe Mines Ltd.). Most recently, in May 2014, Polymetal International PLC (Polymetal) announced acquisition of the Kyzyl Project, of which Bakyrchik is a part of. Polymetal is considering two options before making a choice: processing of ore or concentrate using POX (pressure oxidation) or sale of the concentrate to third parties[15]. The future of the project is, therefore, unclear. A recent independent feasibility study estimated indicated mineral resources of 7.35 Moz (in addition to 5.76 Moz of reserves) at the Bakyrchik deposit[22]. Estimates suggest potential productivity of the Bakyrchik deposit at 10-15 t gold per year for a minimum of 20 years[15].

Currently, the Bakyrchik Mine is on a sustained care and maintenance. The historic mine disturbance and contamination issues are subject to environmental monitoring and reporting. To date only less than 10 % of Bakyrchik ore has been mined. Given the rising demand for precious metals, and the potential growth in their commodity value, it is clear that mining of troublesome ores such as Bakyrchik may be restarted in the near future and existing environmental concerns (from past mine operations) may be exacerbated. An effective and ecologically- favourable extractive methodology must be found urgently.

2 Feasibility of processing Bakyrchik concentrates by direct reductive melting

2.1 Investigations on processing refractory gold-arsenic-bearing Bakyrchik concentrates

For many years, a number of organizations and individual researchers carried out investigations into the development of an improved technology for processing the Bakyrchik ore. The most widespread method employed so far for gold recovery from refractory sulfide raw materials is oxidative roasting followed by cyanidation or thiocarbamide leaching. A number of investigations into the processing of the Bakyrchik concentrate by this method have been carried out[5],[23]. Pilot plant tests of oxidative roasting of Bakyrchik concentrates in two cascaded fluidized bed furnaces with 400 kg/d output defined the optimum regimes for arsenic sublimation, and sulfur and carbon oxidation. Two-stage roasting was carried out at 550 °C and 650 °C with an excess of air, with cakes from the calcine (after cyanidation) containing 22 g/t of Au[24]. Respectable levels of gold recovery were only achieved after carefully following a two-stage roasting method, and by leaching the arsenous films of the calcine with alkaline solutions, using two-stage adsorptive leaching with an ion-exchange resin, and flotation[25]. Melting of the calcine mixed with a furnace charge of molten copper, proved unprofitable, owing to large losses of copper into the slags. Further disadvantages included the complexity of the multi-stage method, incomplete recovery of gold, the presence of arsenic (with the formation of large amounts of toxic white arsenic), the need for expensive dust trapping processes, and problems associated with disposal of toxic waste. The roasting and cyanidation scheme was repeatedly

discussed but never accepted for practical implementation.

At a sulfide metallurgical plant of the Bakyrchik enterprise, tests were carried out on processing ores by the "redox-process". Sobel et al. (1995) describes a redox process employing autoclave leaching of an ore concentrate in nitric acid, with regeneration promoted directly in the autoclave by controlled oxidation in situ [26]. In this process arsenic precipitates from the redox leachate solution residue in the form of the relatively low-toxic compound ferric arsenate. Moreover, it was observed that redox treatment deactivates preg-robbing carbon. Despite this, the redox process has not been pursued beyond pilot testing in Bakyrchik, due to low gold recoveries [21].

One of the promising hydrometallurgical approaches proposed for processing Bakyrchik concentrates is electrosorption leaching of gold, directly from ores and concentrates, using membrane electrolysers [27]. The advantages of this method are that oxidation of sulfides proceeds under the influence of the flow of electric current, without the need for additional reagents at low temperatures, using simple equipment, and partitions arsenic into low-toxic scorodite ($FeAsO_4$). Electrochemical processing conditions for refractory sulphide ores and concentrates were optimized on representative samples of the Bestobe deposit giving more than 96% gold recovery. Unfortunately, larger scale tests on Bakyrchik concentrates were not conducted, so the influence of carbonaceous matter on the process is unclear, and ways to fully remove arsenic as a low-toxic form have not been considered. In view of the above, and taking into account the fact that Bakyrchik is situated in a region with limited water resources, it is important to also be attentive to pyrometallurgical processing methods, especially in view of the refractory nature of the ores and concentrates of the deposit.

Alternative pyrometallurgical methods have been attempted. Dearsenicative roasting of sulfide concentrates with a limited amount of oxygen in a fluid bed furnace, with arsenic sublimation, mainly in the form of sulfides followed by copper matte smelting has been developed and tested [28]. A high degree of arsenic sublimation (98%), mainly as sulfides, can be achieved by oxidizing-sulfidizing roasting of Bakyrchik concentrates [29]. The process takes place in specially constructed shaft furnaces, with subsequent gold recovery by cyanidation after the removal of carbon by oxidative roasting. This technology has been tested on semi-industrial scale. The disadvantages of this method when applied to the Bakyrchik concentrate are the necessity for precise control of oxygen during roasting in order to avoid formation of toxic white arsenic, and complicated schemes for further gold recovery.

One environmentally-friendly method for the dearsenication of refractory sulfide raw materials is vacuum-thermal sublimation, allowing the removal of up to 96-98% of the arsenic in the form of a low-toxic sulfide condensate in a one-stage process, irrespective of the initial arsenic content [30]. The process proceeds in ten minutes at 720-750°C and pressures below 3-5 kPa, in an engineered vibration device which runs continuously. The gases dumped into the atmosphere by the vacuum pump do not require sanitary treatment, because the contents of arsenic and its compounds are much lower than the maximum concentration limit. Pilot plant tests with Bakyrchik and Nezhdaninsk concentrates in a continuously operating vibrovacuum installation at 5 t/d productivity have confirmed high degrees of arsenic sublimation into a low-toxic sulfidic form in one stage. Based on these results, a trial installation working at 10 t/d productivity for processing the gravitational concentrate of the Bakyrchik deposit was created [31]. However, following the transfer of control of the deposit to overseas investors in the 1990s, the installation was dismantled and works were ceased. The shortcomings of this vacuum-thermal scheme of gold processing are the technological challenge of continuously operating the vacuum installation and the complicated scheme of gold extraction from the

subsequent calcine. This is due to the fact that high gold recovery rates can only be reached by matte smelting of the calcine with a copper furnace charge or by cyanidation after removal of carbon to 0.1% and iron to 1%[30,31].

The most recently-tested technology, which recovered at least 88% of the gold of Bakyrchik concentrate, was based on a two-stage fluidized-bed ore roasting followed by processing with a conventional cyanide leaching circuit. Pilot test work was accomplished under the supervision of Crescent Technology and undertaken at Hazen Research's Colorado facilities[16]. Mine production was planned for 2013, however, after aquisition of control of Turquoise Hill Resources Ltd. by Rio Tinto Group, this option was abandoned.

In another study high gold recovery in a lead collector was achieved by alkaline melting of refractory concentrates with NaO and alkalis, resulting in transfer of arsenic to the slag[32]. The main limitations of this method are the large consumption of reagents, complexity in processing the arsenic-bearing slags and corrosion of casting vessels.

Heating of arsenopyrite in a reducing atmosphere in the presence of CO and CO_2 was studied by Chakraborti and Lynch[33]. It was found that the presence of CO_2 can substantially decrease the rate of arsenic removal into the gas phase according to reactions:

$$2\,FeAsS + CO_2\uparrow \longrightarrow FeO + CO\uparrow + AsS\uparrow$$
$$FeAsS + 2\,CO_2\uparrow \longrightarrow FeAs + SO_2\uparrow + 2\,CO\uparrow$$

Chakraborti and Lynch suggested that mixing of an arsenopyrite-bearing material with excess coal and melting the mixture in air could be a potential solution to the problem of arsenic elimination. Aylmore and Lincoln[34] studied mechanochemical milling of arsenopyrite and pyrite in CO_2 atmosphere at room temperature. XRD analysis revealed alteration of arsenopyrite to orthorhombic westerveldite, and some pyrrhotite, probably by the same reaction:

$$FeAsS + 2\,CO_2\uparrow \longrightarrow FeAs + SO_2\uparrow + 2\,CO\uparrow$$

However, no SO_2 has been identified in the gas phase by mass spectroscopic analysis. It has been suggested that SO_2 could have reacted with pyrrhotite by forming pyrite-like phase, which couldn't be detected by XRD due to its low concentrations. Milling of pyrite in the same conditions resulted in formation of pyrrhotite by this reaction:

$$FeS_2 + 2\,CO_2\uparrow \longrightarrow Fe_{1\text{-}x}S + SO_2\uparrow + 2\,CO\uparrow$$

A review of the known methods of processing refractory ores and concentrates demonstrates that feasible solutions exist for preliminary dearsenication of materials, with arsenic removal in the form of low-toxic compounds suitable for long-term storage or disposal. However, many of the methods of processing described are impractical because of their expense and complexity.

Here, we present experiments to develop a new method for gold recovery from refractory gold-arsenic-bearing materials, based on direct reductive melting (DRM) of the concentrate. Compared to the earlier methods used for gold recovery from the Bakyrchik concentrates, this new approach appears more promising[35].

2.2 Thermodynamic modelling of direct reductive melting process

The initial furnace charge of direct reductive melting process consists of the refractory gold-arsenic-bearing Bakyrchik concentrate, litharge, coke, and an iron-containing slag. To define reactions occurring during the melting, thermodynamic modelling was done applying an expanded expression for the Gibbs free energy. This allows calculation of changes in the Gibbs free energy at each of the chemical reactions, and gives their equilibrium constants as a function of temperature[36]. Calculations have been done using the Outokumpu thermochemical suite [37].

$$\Delta G_T^0 = \Delta H_T^0 - T\Delta S_T^0 \tag{1}$$

Input parameters for the calculations were the initial temperature, subsequent polymorphic phase transformations, melting and final temperature. A temperature range of 1023-1523 K, relevant to the proposed melting process, was chosen for the computation of the Gibbs energy. The enthalpy and standard entropy of the components of reactions, coefficients in the heat capacity equations of all reactants, enthalpy and entropy values of any phase transformations and melting temperatures of all components involved in reactions were taken into consideration ((2) and (3)). Reference thermodynamic data of all relevant phases are given in supplementary materials (Table 11).

$$\Delta H_T^0 = \Delta H_{298}^0 + \int_{298}^{T_{tr}} C_{P_1} dT + \Delta H_{tr}^0 + \int_{T_{tr}}^{T_{mel}} C_{P_2} dT + \Delta H_{mel}^0 + \int_{T_{mel}}^{T} C_{P_3} dT \tag{2}$$

$$S_T^0 = S_{298}^0 + \int_{298}^{T_{tr}} \frac{C_{P_1}}{T} dT + \Delta S_{tr}^0 + \int_{T_{tr}}^{T_{mel}} \frac{C_{P_2}}{T} dT + \Delta S_{mel}^0 + \int_{T_{mel}}^{T} \frac{C_{P_3}}{T} dT \tag{3}$$

where: T_{tr} - polymorphic transformation temperature; T_{mel} - melting temperature; C_{P_1}, C_{P_2}, C_{P_3} - heat (thermal) capacities in the corresponding temperature intervals; ΔH_{tr}^0 - enthalpy change at polymorphic transformation; ΔS_{tr}^0 - entropy change at polymorphic transformation; ΔH_{mel}^0 - enthalpy change at melting; ΔS_{mel}^0 - entropy change at melting.

Since the basic mineral constituents of the concentrate are pyrite, arsenopyrite, and quartz, the thermodynamic analysis of the assumed reactions in the FeS_2−FeAsS−SiO_2−CaO−FeO−C−PbO system have been used to predict the most probable reactions in the range of temperatures 1023-1523 K (Table 2).

Calculated values of the Gibbs energy change of possible reactions are summarized in Figure 2. For the calculation it was assumed that sulfur in this temperature interval is in its vapour state (as S_2), and arsenic at 883 K is in the gas state (as As_4)[38].

The calculated values of arsenopyrite dissociation reactions (1-3,7) are significantly negative and strongly indicate that dissociation should occur. Comparison of the magnitudes of Gibbs energy changes leads to the conclusion that reaction (3) is the most preferred. Arsenic in the gaseous state exists in the form of As_4, As_2 and As_4S_4. It can be seen from the tabulated data that, in the presence of carbon, the stability of arsenopyrite and pyrite (reactions 7,8) are significantly decreased compared to reactions (1) and (6). In the presence of carbon and CaO, the change of Gibbs energy for the reaction (12) of calcium oxide with iron sulfide, formed by the dissociation of arsenopyrite and pyrite, also has much greater negative value compared to reaction (13). The possibility of further dissociation of the $FeAs_2$, formed by the reaction

Table 2: Modelled reactions in the FeS_2−FeAsS−SiO_2−CaO−FeO−C−PbO system

№	Reaction
	Dissociation of arsenopyrite and pyrite
1.	$4\,FeAsS = 4\,FeS + As_4$
2.	$6\,FeAsS = 6\,FeS + As_4 + As_2$
3.	$16\,FeAsS = 4\,FeAs_2 + 12\,FeS + As_4S_4 + As_4$
4.	$4\,FeAs_2 = 4\,FeAs + As_4$
5.	$8\,FeAs = 4\,Fe_2As + As_4$
6.	$2\,FeS_2 = 2\,FeS + S_2$
7.	$4\,FeAsS + 4\,CaO + 4\,C = 4\,CaS + 4\,Fe + As_4 + 4\,CO$
8.	$FeS_2 + 2\,CaO + 2\,C = 2\,CaS + Fe + 2\,CO$
	Reduction of iron
9.	$CaO + 0.75S_2 = CaS + 0\cdot 5\,SO_2$
10.	$FeO + 0.75S_2 = FeS + 0\cdot 5\,SO_2$
11.	$2\,FeO\cdot SiO_2 + 2\,CaS = 2\,CaO\cdot SiO_2 + 2\,FeS$
12.	$CaO + FeS + C = CaS + Fe + CO$
13.	$CaO + FeS = CaS + FeO$
14.	$FeO + C = Fe + CO$
	Formation of iron-arsenic alloy
15.	$As_2 + Fe = FeAs_2$
16.	$As_4 + 2\,Fe = 2\,FeAs_2$
17.	$As_2 + 2\,Fe = 2\,FeAs$
18.	$As_4 + 4\,Fe = 4\,FeAs$
19.	$As_2 + 4\,Fe = 2\,Fe_2As$
20.	$As_4 + 8\,Fe = 4\,Fe_2As$
21.	$As_4 + 2\,S_2 = As_4S_4$
22.	$As_4 + 3\,O_2 = 2\,As_2O_3$
23.	$2\,As_2O_3 + 6\,C = As_4 + 6\,CO$
	Reduction of litharge
24.	$PbO + C = Pb + CO$
25.	$PbO + CO = Pb + CO_2$
26.	$PbO + Fe = Pb + FeO$

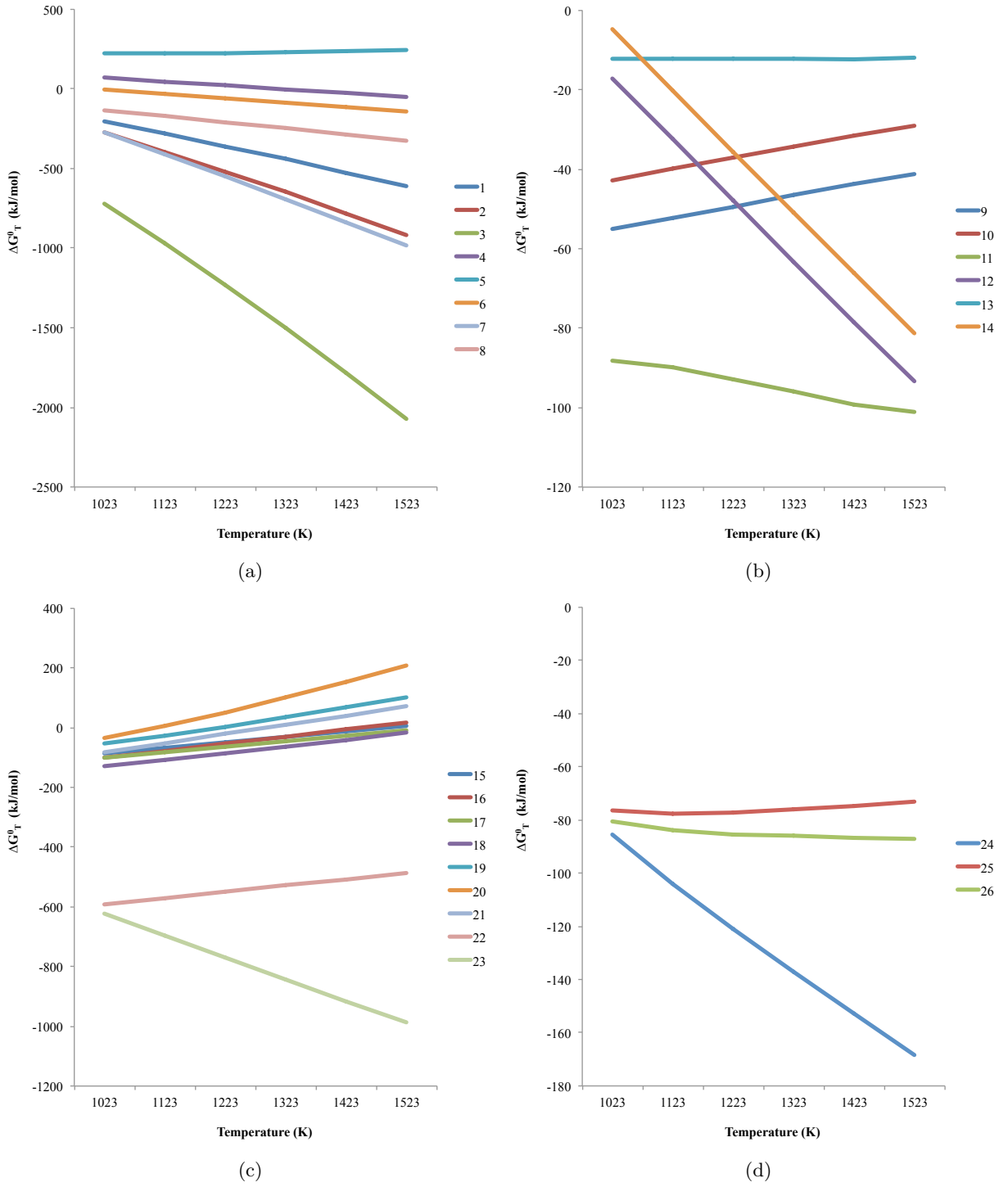

Figure 2: Variation of the Gibbs energy changes of the reactions in $FeS_2-FeAsS-SiO_2-CaO-FeO-C-PbO$ system: (a) dissociation of arsenopyrite and pyrite, (b) reduction of iron, (c) formation of iron-arsenic alloy, (d) reduction of litharge.

(3) is weak and becomes relevant only at temperatures above 1323K. The sulfidation (reactions 9,10) of calcium and iron oxides by elemental sulfur, formed during pyrite dissociation, is also possible. Iron oxide can be reduced by carbon to metallic iron (reaction 14). The interaction of iron silicate with calcium sulfide, when it appears in the system (11), is also possible. As for reactions (15-20), formation of iron arsenides is possible at relatively low temperatures and it may be assumed that reaction (18) proceeds in preferance, as evidenced by the shift of Gibbs energy change to more negative values as temperature increases. Reactions of sulfidation and oxidation of metallic arsenic with formation of sulfide and oxide (reaction 21, 22), and arsenic oxide reduction by carbon (reaction 23) are also possible in the vapour phase. Looking at the results for lead oxide reduction, it can be concluded that reactions 24-26 are feasible at all temperatures. Here, the most negative value of Gibbs energy change, and therefore the greatest thermodynamic driving force, is associated with the interaction between lead oxide and carbon (reaction 24). Litharge can be reduced either by carbon or metallic iron (reaction 26).

The thermodynamic calculations therefore allow us to predict the most probable interactions proceeding during direct reductive melting of Bakyrchik gold-arsenic-bearing concentrates over a range of temperatures from 1023 to 1523 K.

$$6\,\mathrm{FeAsS} = 6\,\mathrm{FeS} + \mathrm{As_4} + \mathrm{As_2}$$
$$16\,\mathrm{FeAsS} = 4\,\mathrm{FeAs_2} + 12\,\mathrm{FeS} + \mathrm{As_4S_4} + \mathrm{As_4}$$
$$4\,\mathrm{FeAsS} + 4\,\mathrm{CaO} + 4\,\mathrm{C} = 4\,\mathrm{CaS} + 4\,\mathrm{Fe} + \mathrm{As_4} + 4\,\mathrm{CO}$$
$$4\,\mathrm{FeAs_2} = 4\,\mathrm{FeAs} + \mathrm{As_4}$$
$$\mathrm{FeS_2} + 2\,\mathrm{CaO} + 2\,\mathrm{C} = 2\,\mathrm{CaS} + \mathrm{Fe} + 2\,\mathrm{CO}$$
$$2\,\mathrm{FeO}\cdot\mathrm{SiO_2} + 2\,\mathrm{CaS} = 2\,\mathrm{CaO}\cdot\mathrm{SiO_2} + 2\,\mathrm{FeS}$$
$$\mathrm{CaO} + \mathrm{FeS} + \mathrm{C} = \mathrm{CaS} + \mathrm{Fe} + \mathrm{CO}$$
$$\mathrm{FeO} + \mathrm{C} = \mathrm{Fe} + \mathrm{CO}$$
$$\mathrm{As_4} + 2\,\mathrm{Fe} = 2\,\mathrm{FeAs_2}$$
$$\mathrm{As_4} + 4\,\mathrm{Fe} = 4\,\mathrm{FeAs}$$
$$\mathrm{As_2} + 4\,\mathrm{Fe} = 2\,\mathrm{Fe_2As}$$
$$\mathrm{PbO} + \mathrm{C} = \mathrm{Pb} + \mathrm{CO}$$

These reactions lead to dissociation of pyrite and arsenopyrite releasing As, fixation of arsenic by Fe reduced from slag with formation of solid iron-arsenide phases, and concentration of gold into lead reduced from litharge.

3 Gold recovery optimisation and arsenic removal

3.1 Materials and methods

Characterisation of the Bakyrchik concentrate. We obtained two batches of gold-arsenic bearing flotation concentrates of Bakyrchik deposit: BC1 and BC2. The concentrates were dark grey in appearance. The water content of the concentrates was determined by thermogravimetric methods by heating at 100 °C and 0.13 kPa until sample weight stopped changing. The average water content of the concentrate samples was found to be 8-10 wt %.

The Bakyrchik concentrates were thoroughly mixed and average specimens were selected by quartering. The bulk chemical composition of the concentrates was determined by ICP-MS. The principal constituents are shown in Table 3. The gold content was analyzed by fire assay and total sulfur content was determined by the Leco method.

Table 3: Chemical composition of Bakyrchik concentrates

BC1	%	Al	Ca	Fe	K	Mg	Na	P	S	Ti
		0.24	0.48	12.00	0.09	0.33	0.01	0.043	9.73	<0.01
	ppm	Au	Zn	Ag	As	Cu	Mn	Pb	Sb	Sr
		45.00	282	11	48352	496	7386.6	166	7171	150
BC2	%	Al	Ca	Fe	K	Mg	Na	P	S	Ti
		0.31	0.72	9.60	0.11	0.30	0.05	0.05	7.24	<0.01
	ppm	Au	Zn	Ag	As	Cu	Mn	Pb	Sb	Sr
		110	853	2	34935	498	7359.8	729	7500	143

For powder X-ray diffraction data collection BC1 and BC2 samples were ground into a fine powder. The sample holder was a 2 mm thick flat Al holder. Measurements were collected at room temperature in the angular range 10-120° 2θ using a Bruker D8 Advance X-ray diffractometer operating with CuKα1(λ = 1.5406 Å) radiation. The powder patterns were refined by the Rietveld method with the GSAS-EXPGUI package[39,40], using a pseudo-Voigt peak shape function[41] with an asymmetry correction[42]. The raw data were converted into GSAS format for input into EXPGUI using ConvX[43].The crystallographic data used for the input were taken from ICSD database[44] and are given in supplementary materials. During Rietveld refinement, background coefficients, zero-shift error, cell parameters, peak shape parameters, preferred orientation with correction via the March-Dollase algorithm[45] and phase fractions were optimized for each phase. Rietveld refinements of the PXRD patterns of the Bakyrchik concentrates are given as supplementary material (Fig. 10). The results of quantitative phase analysis are given in Table 4.

Table 4: PXRD quantitative phase analysis of Bakyrchik concentrate, wt.%.

Sample	Quartz	Sericite	Graphite	Muscovite	Pyrite	Arsenopyrite	Wollastonite
BC1	10.35	58.47	8.12	8.2	9.4	0.84	4.46
BC2	15.78	61.65	2.38	9.08	6.83	0.98	3.26

Experimental design. In order to define optimum conditions for gold extraction into lead and arsenic extraction into iron-arsenic alloy, the distribution of metals, depending on melting conditions, fusion mixture composition and other physical parameters have been investigated. We have used a method of probabilistic-deterministic planning of experiments[46,47] to determine the optimal parameters of the DRM process of Bakyrchik concentrates. This method allows us to obtain the optimum conditions for DRM of Bakyrchik concentrates in the form of multifactorial equations related to the extraction rate of gold in draft lead, and arsenic in iron-arsenic alloy. The model will provide the optimum technological parameters for the process.

Gold extraction from concentrate into the crude lead and arsenic removal into the iron-arsenic alloy has been studied depending on some of the most important for the process parameters: temperature, holding time, the content of lead oxide, slag iron and coke in the fusion mixture. The matrix consisted of 25 experiments. The parameters ($x_i, i = 1 - 5$) and their values are shown in Table 5.

Table 5: Studied parameters and their values

Parameters	Parameter value				
	1	2	3	4	5
x_1, temperature, °C	850	950	1050	1150	1250
x_2, holding time, h	1	1.5	2	2.5	3
x_3, content of PbO by weight of the concentrate, %	20	30	40	50	6
x_4, content of Fe in slag by weight of the concentrate, %	20	25	30	35	40
x_5, content of C by weight of the concentrate, %	2	6	10	14	18

The experimental design was such that during all experiments each value of any parameter meets once with each value of all the other parameters. This ensures the effect that could be achieved with an infinitely large number of experiments with random variation of the parameters.

Data processing. The yield of gold and arsenic extraction was calculated according to equation (4) (unit fraction):

$$Y_e = \frac{Me_{prod} \times m_{prod}}{Me_{init} \times m_{init}} \tag{4}$$

where: Me_{prod} - metal content in relevant melting product, %; m_{prod} - mass of the relevant melting product, g; Me_{init} - metal content in initial sample, %; m_{init} - mass of the sample, g.

The experimental data have been used to construct curves of metal yield into the corresponding products for a given space of investigated parameters. Constructing the curves is necessary to determine the analytical form of the dependence. A method of least squares is the most common way to select the approximation function. After finding the analytical form of the dependence, we calculated its parameters. The significance level of the correlation coefficient and adequacy of the model, and hence of the verifiable dependency for 95% significance level is determined by the inequality (5):

$$t_R = \frac{R\sqrt{N - K - 1}}{1 - R^2} > 2 \tag{5}$$

using nonlinear multiple correlation coefficient R (6):

$$R = \sqrt{1 - \frac{(N-1)\sum_{i=1}^{N}(Yei - Yti)^2}{(N-K-1)\sum_{i=1}^{N}(Yei - Yav)^2}} \tag{6}$$

where: N - the number of points, K - the number of active parameters, Yei - an experimental value of the result, Yti - a calculated value, Yav - an average experimental value.

Based on the significant correlations (5) generalized multivariate equations for the extraction of gold and arsenic were created using (7):

$$Y_P = \frac{\prod_{n=i}^{k} Y_i}{Y_{av}^{k-1}} \tag{7}$$

where Y_P - generalized function, k - number of parameters, Y_i - individual parameters, $\prod$ - product of all functions, Y_{av} - average of all the accounted results of the experiment.

The error is calculated as (8):

$$\sigma = \sqrt{\frac{\sum_{i=1}^{N}(Yei - Yti)^2}{(N - K - 1)}} \tag{8}$$

3.2 Results

Starting materials were a gold-arsenic bearing Bakyrchik concentrate, containing: Au - 45 g/t, As - 8.2%, S - 19.0%; lead oxide (analytical grade); coke (reducing agent, 85% C); iron-rich waste slag (from lead melting) containing, weight %: 32.1 Fe, 27.5 SiO_2, 10.8 Al_2O_3, 22.3 CaO, 2.2 MgO, 0.1 Pb, 1.46 Zn. A mix of 50 g of the concentrate was prepared with lead oxide, coke, and a top fill of a slag layer. Melting has been conducted in a reduced atmosphere. Carbon in the form of coke has been added to the furnace charge in order to generate reducing conditions (CO and CO2):

$$C + O_2 = CO_2$$
$$CO_2 + C = CO$$

The fusion mixture was placed in a corundum crucible and melted at 1200 °C for 2 hours. Experiments have been conducted using a laboratory electric shaft furnace SSHOL -1.1.6 / 12 M3. The furnace is a rectangular body made from sheet steel. It comprises a heating chamber and a control unit. The heating chamber consists of a ceramic flange, a heater, a hearth, a ring and an insulation. The heater is designed as a ceramic tube in which a wire of resistance alloy is fixed by high alumina daubing. The inner surface of the heater tube is a workspace of the furnace. The workspace is closed by a lid to reduce heat loss. A control unit of the furnace automatically maintain the desired temperature with an accuracy of ±1.5°C. Elements of the control unit are regulator-millivoltmeter, an electronic console, a thyristor, a warning light and a switch. They all are located on a front panel, which is mounted on the side walls of the heating chamber by four screws. Temperature control is carried out by platinum-platinum-rhodium thermocouple.

The crucible was smashed after cooling. The charge had divided into three layers - the top slag, an iron-arsenic alloy, and the lead bullion at the base. Products were separated and weighed. The iron-arsenic alloy was analysed for arsenic by ICP-MS, the lead and slag were analysed for gold using a fire assay. A sample of resultant waste slag, obtained by the DRM, contained, in weight %: 0.08 As; 0,1 S; 6,4 Fe; 31.18 SiO_2; 11.66 Al_2O_3; 11.36 CaO; 1.38 MgO; 0.04 Cu; 0.99 K_2O; 0.9 Pb; 0.86 Zn; 2 g/t Au and 20 g/t Ag.

The plan-matrix and results of the experiments are shown in Table 6. The results of the experiments show that gold recovery into lead ranged from 25.03 to 94.98%, and arsenic extraction into the alloy varied from 42.6 to 94.12%. The metals' yields into the corresponding products as a function of the investigated parameters are shown in Figure 3.

Table 6: A matrix of five-factorial experiment at five levels

Exp-t	x_1,°C	x_2,h	x_3,%	x_4,%	x_5,%	Au into crude Pb,%		As into Fe-As alloy,%	
						Yexp	Ycalc	Yexp	Ycalc
1	850	1	20	20	2	25.03	37.30	42.6	51.03
2	850	2	40	30	10	66.28	60.65	86.52	84.04
3	850	1.5	30	25	6	48.97	50.32	85.03	69.57
4	850	3	60	40	18	66.12	67.95	89.13	92.42
5	850	2.5	50	35	14	60.87	66.85	87.86	92.08
6	1050	1	40	25	18	65.18	76.42	74.23	69.80
7	1050	2	30	40	14	85.23	78.44	92.6	94.92
8	1050	1.5	60	35	2	58.17	57.41	65.38	77.09
9	1050	3	50	20	10	87.12	85.63	60.3	61.83
10	1050	2.5	20	30	6	48.88	64.16	63.05	80.40
11	950	1	30	35	10	65.35	61.27	93.5	83.38
12	950	2	60	20	6	61.08	62.49	64.61	59.90
13	950	1.5	50	30	18	72.01	71.37	90.3	82.43
14	950	3	20	25	14	81.07	68.18	89.5	75.06
15	950	2.5	40	40	2	56.74	55.34	94.12	82.17
16	1250	1	60	30	14	93.79	92.76	62.51	79.12
17	1250	2	50	25	2	81.29	74.92	64.41	65.80
18	1250	1.5	20	40	10	72.93	80.69	87.6	90.81
19	1250	3	40	35	6	80.48	94.05	69.01	84.58
20	1250	2.5	30	20	18	94.98	97.27	61.26	63.49
21	1150	1	50	40	6	81.93	74.31	92.5	82.23
22	1150	2	20	35	18	92.02	79.97	91.05	90.79
23	1150	1.5	40	20	14	91.08	88.37	50.63	62.28
24	1150	3	30	30	2	79.11	68.66	80.01	72.62
25	1150	2.5	60	25	10	92.79	90.05	85.67	75.19

Note: Error of equation (9), abs. %: $\sigma = 8.76$. Correlation coefficient at $N = 25$ and $K = 5$: $R = 0.86$, $t_R = 14.4 > 2$. Error of equation (10), abs. %: $\sigma = 10.97$. Correlation coefficient at at $N = 25$ and $K = 5$: $R = 0.69$, $t_R = 5.74 > 2$.

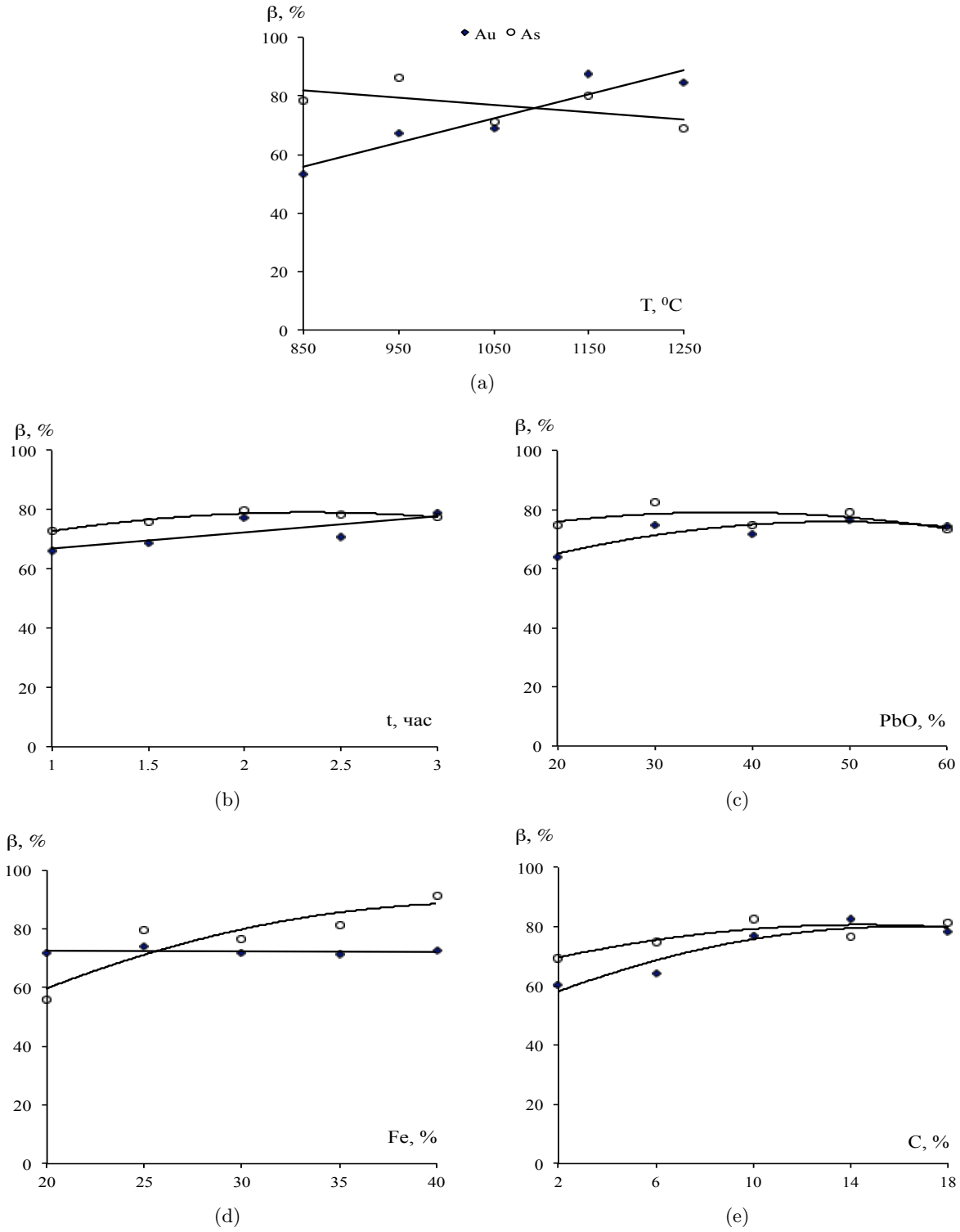

Figure 3: Gold extraction into the crude lead and arsenic extraction into the iron-arsenic alloy as a function of: a) temperature, b) holding time, c) the content of lead oxide in the fusion mixture, d) the content of iron in the fusion mixture, and e) the content of coke in the fusion mixture

Gold extraction into the lead increases with the increasing temperature, holding time, the content of litharge and coke in the furnace charge. The amount of iron has almost no effect on the recovery of gold. Additives of lead oxides in the fusion mixture of more than 50% by weight of the concentrate are impractical due to the large consumption of the expensive reagent. Using less than 30% PbO additive is also economically inefficient because of possible reduction of the gold extraction into metal lead.

With increasing temperature and holding time the arsenic recovery into the iron-arsenic alloy decreases, probably due to a gradual decomposition of the iron arsenides and formation of gaseous arsenic by the following reactions[48]:

$$\mathrm{FeAs_2} \xrightarrow{528\text{-}680^\circ\mathrm{C}} \mathrm{FeAs_{1.5}} + \tfrac{1}{8}\,\mathrm{As_4}\uparrow$$
$$\mathrm{FeAs_{1.5}} \xrightarrow{680\text{-}850^\circ\mathrm{C}} \mathrm{FeAs} + \tfrac{1}{8}\,\mathrm{As_4}\uparrow$$
$$2\,\mathrm{FeAs} \xrightarrow{>850^\circ\mathrm{C}} \mathrm{Fe_2As} + \tfrac{1}{2}\,\mathrm{As_2}\uparrow$$

By increasing the amount of iron in the furnace charge we can significantly increase the extraction of arsenic into the alloy, which is apparently associated with the formation of a more stable lower arsenic-content arsenide Fe_2As. Elevated temperatures and the content of litharge in the fusion mixture do not seem to have a noticeable effect on the extraction of arsenic into the alloy.

Table 7 shows the correlation coefficients R and their significance for functions Y_i. In our experiments the linear dependence Y_4 was not significant for gold extraction and it has been excluded from the further consideration. Dependencies Y_1 and Y_3 were found to be insignificant for arsenic, and have also been excluded.

Table 7: Functions, correlation coefficients, and their significance

Y_i	R	tR	Function significance
Au into crude Pb			
$Y_1 = 0.0826x_1 - 14.407$	0.94	13.86	significant
$Y_2 = 5.4536x_2 + 61.433$	0.79	3.73	significant
$Y_3 = -0.0132x_3^2 + 1.2858x_3 + 44.726$	0.88	6.75	significant
$Y_4 = -0.0204x_4 + 72.951$	0.17	0.30	insignificant
$Y_5 = -0.1081x_5^2 + 3.5143x_5 + 51.46$	0.95	17.06	significant
As into Fe-As alloy			
$Y_1 = -0.025x_1 + 103.16$	0.56	1.42	insignificant
$Y_2 = -3.5829x_2^2 + 16.661x_2 + 59.736$	0.95	18.39	significant
$Y_3 = -0.0107x_3^2 + 0.7924x_3 + 64.42$	0.59	1.56	insignificant
$Y_4 = -0.05698x_4^2 + 4.86321x_4 - 14.82743$	0.90	8.47	significant
$Y_5 = -0.071x_5^2 + 2.0586x_5 + 65.718$	0.85	5.47	significant

Based on the significant functions (Table 7) generalized multivariate equations for the extraction of gold (9) and arsenic (10) were composed using expression (7):

$$\beta_{\mathrm{Au}} = 2.64 \times 10^{-6}(0.083t^2 - 14.41) \times (5.45\tau + 61.43) \times (-0.013C_{PbO}^2 + 1.286C_{PbO} + 44.73)\times \\ \times(-0.108C_C^2 + 3.51C_C + 51.46) \tag{9}$$

$$\beta_{\mathrm{As}} = 1.68 \times 10^{-4}(-3.583\tau^2 + 16.661\tau + 59.736) \times (-0.057C_{Fe}^2 + 4.863C_{Fe} - 14.827)\times \\ \times(-0.071C_C^2 + 2.059C_C - 65.718) \quad (10)$$

where: t - temperature, °C; τ - holding time, h; C_{PbO} - PbO content by weight of the concentrate, %;C_{Fe} - Fe content by weight of the concentrate, %; C_C - C content by weight of the concentrate, %.

Optimal conditions for the extraction metals into the relevant melting products have been calculated using equations (9) and (10). The high gold recovery into lead (97%) is reached at the following optimal conditions: 1250 °C temperature; 2.5 h of holding time; litharge content in the fusion mixture - 30%, and coke - 18% by weight of the concentrate. Optimum conditions for the extraction of arsenic into the iron-arsenic alloy (95%) are as follows: holding time of two hours; an iron content (in the slag) of 40% by weight of the concentrate, and coke - 14-18% by weight of the concentrate. To implement the whole process whilst ensuring complete separation of gold and arsenic at 1150-1250 °C, a relatively high rate of iron is required for binding the arsenic, which results from the decomposition of higher iron arsenides to lower iron arsenide.

Proposed technological scheme of the DRM process is shown in Figure 4. During the DRM, arsenopyrite in the gold-arsenic bearing concentrate dissociates with production of elementary arsenic. Arsenic further reacts with iron, resulting from the reduction of slag, and forms iron-arsenic alloy. Lead oxide is reduced to metal, which concentrates gold. The iron-arsenic alloy forms a separate phase. The alloy is practically insoluble in molten lead, floats to the surface and lies directly above the molten lead. During flushing of products from the furnace it can be easily separated from the lead and slag.

The gold bearing lead can be transferred to the cupellation furnace where it is oxidised. The lead oxides produced are then can be returned for re-use in the early stage of the DRM process. Hence, the annual consumption of the litharge will be determined by the replenishement of the loss of lead with DRM products. The gold-silver alloy, obtained from the cupellation (so called Dore's metal) is a saleable output.

3.3 Environmental aspects.

Environmental concerns related to the DRM process are lead handling, and potential vaporised arsenic. Since litharge is a powder material, to avoid flue dust loss, and subsequent lead contamination, a furnace charge should be in a granular form. Also, trapped lead-containing dust should be returned to the furnace charge to minimize lead losses.

In the lab experiments, a composition of generated gases has not been determined. However, we observed condensation of AsS and S in the gas-outlet flue. This is consistent with data of Chakraborti and Lynch [33], who investigated the thermodynamics of arsenopyrite roasting by heating synthetic and natural arsenopyrite in reducing, oxidising, and neutral media at temperatures ranging from 525 to 600 °C. In their experiment under neutral conditions, arsenic was removed as As_4 vapour, and a solid product was found to be FeS. Albeit admitting absence of As-S liquid in their study, they did not exclude the possibility of formation of As-S liquid phase under real hearth roasting conditions, which is shown in phase diagrams for the S-As system at 525°C developed by Barton et al., 1969 [49].

Heating of arsenopyrite in a reducing atmosphere in the presence of CO and CO_2 was studied by Chakraborti and Lynch [33]. It was found that in reducing conditions As_4S_4 is more responsible for arsenic removal rather than As_4. Oxygen present in the system reacts with iron, forming a solid phase that consisted of FeO and Fe_3O_4. The authors also noted that compared to roasting in neutral media, the addition of CO_2

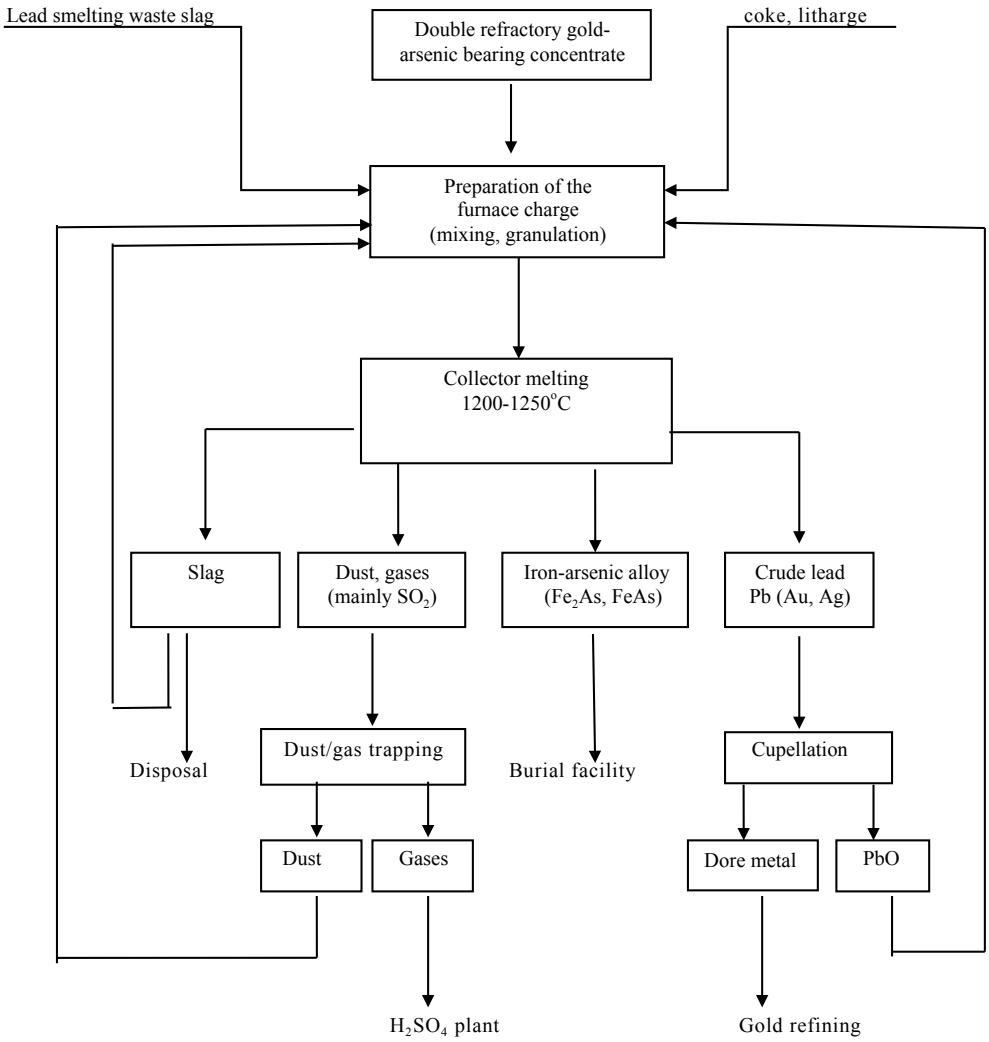

Figure 4: Proposed technological scheme of the DRM process.

into the gas phase substantially reduced the rate of arsenic removal from 60 to 23% with a CO_2/CO ratio of 20. A further decrease in arsenic removal to 15% was reached with a CO_2/CO ratio of 50 in the gas media. Overall, the process was explained by following reactions:

$$2\,\mathrm{FeAsS} + \mathrm{CO_2}\uparrow \longrightarrow \mathrm{FeO} + \mathrm{CO}\uparrow + \mathrm{AsS}\uparrow \tag{11}$$

$$4\,\mathrm{FeAsS} + 4\,\mathrm{CO_2}\uparrow \longrightarrow 4\,\mathrm{FeO} + 4\,\mathrm{CO}\uparrow + \mathrm{As_4S_4}\uparrow \tag{12}$$

$$3\,\mathrm{FeAsS} + 2\,\mathrm{CO_2}\uparrow \longrightarrow 2\,\mathrm{Fe} + \mathrm{FeAs} + 2\,\mathrm{CO}\uparrow + \mathrm{As_2S_3}\uparrow \tag{13}$$

$$\mathrm{FeAsS} + 2\,\mathrm{CO_2}\uparrow \longrightarrow \mathrm{FeAs} + \mathrm{SO_2}\uparrow + 2\,\mathrm{CO}\uparrow \tag{14}$$

$$\tag{15}$$

Depending on the partial pressure of As_4 in the system, FeAs might be replaced by $FeAs_2$ or Fe_2As. It has been concluded that retaining the arsenic in the solid phase by these reactions in reducing media might be a key to the problem of arsenic removal from the raw materials.

In our experiments, the amount of the condensed phases and dusts was around 0.5-1.0%, the remainder apparently relates to non-condensable gases, such as SO_2, CO and CO_2. According to the lab results, only a small amount of arsenic can pass to the gas phase in the form of sulfides. At the industrial scale, if arsenic oxidation occurs due to flue leakage, it can be captured by the existing gas handling systems, and further stabilisation/solidification.

4 Identification and characterization of iron-arsenic alloy.

4.1 Iron arsenides

Iron arsenides may be the key to extraction of gold from existing refractory ores such as that at Bakyrchik. In the course of the DRM process iron arsenides may be formed during arsenopyrite dissociation, and from interaction of arsenic with iron reduced from slag. Literature contains data on the behaviour of arsenopyrite during heating in various atmospheres. However, there is no single point of view on the mechanism of arsenopyrite dissociation.

According to Strathdee and Pidgeon, 1961 [50] upon heating in neutral media, arsenopyrite decomposes with formation of a solid residue, comprising iron sulfides - pyrrhotine and troilite. Zhuchkov et al., 1967 [51] reported similar behaviour of arsenopyrite heated in neutral atmosphere:

$$4\,\mathrm{FeAsS} \longrightarrow 4\,\mathrm{FeS} + \mathrm{As_4} \tag{16}$$

This was proven by Chakraborti and Lynch [33]. Under neutral conditions and at temperature range of 525 - 600 °C, arsenic was removed from arsenopyrite as As_4 vapour, and a solid product was found to be FeS. Later works on the thermal dissociation of natural arsenopyrite in neutral atmospheres [52,53] differ from those aforementioned by the presence of iron arsenides in the intermediate and final solid products of thermal dissociation of natural arsenopyrite.

The research conducted most recently by Khrapunov and co-authors in 1991 [54] indicates the stepwise mechanism of arsenopyrite decomposition. Natural and synthetic arsenopyrite were heated at 10°/min in vacuum and neutral environments and analysed using mass spectrometry and Mössbauer spectroscopy. In both vacuum and neutral environments the compositions of the solid residues were identical, and contained

FeS, FeS_{1-x}, and Fe_2As. The following mechanism of decomposition was proposed:

$$2\,FeAsS \xrightarrow{>300^{\circ}C} FeAs_2 + FeS_2 \tag{17}$$

$$FeAs_2 \xrightarrow{520\text{-}680^{\circ}C} FeAs_{1.5} + \tfrac{1}{8}\,As_4 \tag{18}$$

$$FeAs_{1.5} \xrightarrow{680\text{-}850^{\circ}C} FeAs + \tfrac{1}{8}\,As_4 \tag{19}$$

$$2\,FeAs \xrightarrow{850\text{-}950^{\circ}C} Fe_2As_{1+x} + \frac{1-x}{2}As_2 \tag{20}$$

$$Fe_2As_{1+x} \xrightarrow{1100\text{-}1200^{\circ}C} Fe_2As_{1-y} + \frac{x+y}{2}As_2 \tag{21}$$

$$FeS_2 \xrightarrow{620\text{-}800^{\circ}C} FeS + \tfrac{1}{2}\,S_2 \tag{22}$$

$$FeS \xrightarrow{>1100^{\circ}C} FeS_{1-x} + \frac{x}{2}S_2 \tag{23}$$

$$2\,FeAs_2 + S_2 \rightleftharpoons FeS + As_4 \tag{24}$$

$$4\,FeAs + 2\,S_2 \rightleftharpoons 4\,FeS + As_4 \tag{25}$$

$$2\,Fe_2As + 4\,S_2 \rightleftharpoons 8\,FeS + As_4 \tag{26}$$

$$\frac{n}{4}As_4 + \frac{m}{2}S_2 \rightleftharpoons As_nS_m. \tag{27}$$

Heating of arsenopyrite in a reducing atmosphere in the presence of CO and CO_2 was studied by Chakraborti and Lynch [33]. It was found that in reducing conditions As_4S_4 is more responsible for arsenic removal rather than As_4. Oxygen present in the system reacts with iron, forming a solid phase that consisted of FeO and Fe_3O_4. The authors also noted that compared to roasting in neutral media, the addition of CO_2 into the gas phase substantially reduced the rate of arsenic removal from 60 to 23% with a CO_2/CO ratio of 20. A further decrease in arsenic removal to 15% was reached with a CO_2/CO ratio of 50 in the gas media. Overall, the process was explained by following reactions:

$$2\,FeAsS + CO_2\uparrow \longrightarrow FeO + CO\uparrow + AsS\uparrow \tag{28}$$

$$4\,FeAsS + 4\,CO_2\uparrow \longrightarrow 4\,FeO + 4\,CO\uparrow + As_4S_4\uparrow \tag{29}$$

$$3\,FeAsS + 2\,CO_2\uparrow \longrightarrow 2\,Fe + FeAs + 2\,CO\uparrow + As_2S_3\uparrow \tag{30}$$

$$FeAsS + 2\,CO_2\uparrow \longrightarrow FeAs + SO_2\uparrow + 2\,CO\uparrow \tag{31}$$

$$\tag{32}$$

Depending on the partial pressure of As_4 in the system, FeAs might be replaced by $FeAs_2$ or Fe_2As. It has been concluded that retaining the arsenic in the solid phase by these reactions in reducing media might be a key to the problem of arsenic removal from the raw materials.

In contrast, heating of arsenopyrite in oxidising conditions up to 1000°C completely transfers As into the gas phase through formation of iron arsenate intermediates [51].

$$FeAsS \xrightarrow{480\text{-}540^{\circ}C} FeS \xrightarrow{500\text{-}600^{\circ}C} Fe_3O_4 \xrightarrow{600\text{-}700^{\circ}C} \gamma - Fe_2O_3 \longrightarrow \alpha - Fe_2O_3 \tag{33}$$

$$FeAsS \xrightarrow{500\text{-}800^{\circ}C} \Phi_1 \xrightarrow{750\text{-}900^{\circ}C} Fe_4As_2O_{11} \xrightarrow{850\text{-}950^{\circ}C} \Phi_2 \xrightarrow{>940^{\circ}C} Fe_2O_3 + As_2O_3(g) \tag{34}$$

The Fe-As system was thoroughly reviewed by Okamoto [58]. According to the phase equilibria the following arsenides can be formed: Fe_2As, Fe_3As_2, FeAs and $FeAs_2$ [58]. The melting points of $FeAs_2$, FeAs, and Fe_2As are 1020, 1030, and 919 °C, respectively. Crystallogrpahic data of compounds and terminal phases of the Fe-As system are presented in Table 8.

Table 8: Crystallographic data[a]

Phase	Chemical formula	Space group	ICSD collection code	Reference
αAs	αAs	$R\bar{3}m$	16516	[59]
Iron diarsenide	$FeAs_2$	Pnnm	94062	[60]
Iron arsenide	FeAs	Pna21	15009	[61]
Diiron arsenide	Fe_2As	P4/nmm	415628	[62]
αFe	αFe	$Im\bar{3}m$	53802	[63]
γFe	γFe	$Fm\bar{3}m$	53449	[64]

Note: [a] no crystallographic data were reported for high-temperature phase Fe_3As_2.

Information on the thermal behaviour of iron arsenides in reducing and neutral atmospheres is very limited. Earlier study on the thermal behaviour of natural loellingite ($FeAs_2$) at 450-800°C and atmospheric pressure reported that loellingite decomposes with the release of arsenic, and formation of FeAs [50]. The thermal behaviour of synthetic iron arsenides in a vacuum (<0.0106 kPa) was studied by Tkach et al., 1977 [55]. Heating of the 0.074-0.14 mm grain sized material at 10°/min rate suggested the following mechanism of decomposition:

$$FeAs_2 \xrightarrow{>700^\circ C} FeAs \xrightarrow{>900^\circ C} Fe_2As. \tag{35}$$

Thorough investigation of thermal behaviour of iron arsenides $FeAs_2$ and FeAs in vacuum has been conducted previously [48]. Arsenides were prepared by sintering a mixture of metallic arsenic and iron in evacuated quartz ampoules. The resulting synthetic iron diarsenide, according to the mineralogical and X-ray structure analysis, contained about 10% of FeAs and corresponded to a formula unit of $Fe_{1.05}As_{1.95}$. The synthesized iron monoarsenide contained about 2% $FeAs_2$. An exothermic peak at 320 to 350°C and an endothermic effect at 650-640°C, accompanied by loss in weight, was observed on the thermogram of $FeAs_2$. The endothermic effect was associated with the decomposition of iron diarsenide. The thermogram of FeAs had an exothermic peak at 340-360°C and the endothermic peak at 630-650°C, accompanied by a slight decrease of mass. A noticeable loss of weight was observed at 820-830°C. PXRD and EPMA of the solid products of monoarsenide decomposition at temperatures above 800°C revealed the presence of Fe_2As. Diarsenide dissociation was investigated by *in-situ* high temperature X-ray diffraction when heating in a vacuum of 0.1 Pa at a temperature range of 25-900°C. X-ray patterns were taken every 50 to 100°C. It was found that $FeAs_2$ decomposition starts at 400°C and ends at 600°C with formation of FeAs. Visible decomposition of FeAs was observed at 650°C and was completed above 800°C with the formation of diiron arsenide Fe_2As in solid-phase. The authors came to the conclusion that the thermal dissociation of iron

diarsenide in a vacuum has stepwise nature:

$$FeAs_2 \xrightarrow{510\text{-}690^\circ C} FeAs_{1.5} + \tfrac{1}{8}\, As_4 \uparrow \quad (36)$$

$$FeAs_{1.5} \xrightarrow{690\text{-}805^\circ C} FeAs + \tfrac{1}{8}\, As_4 \uparrow \quad (37)$$

$$FeAs \xrightarrow{805\text{-}1200^\circ C} FeAs_{0.5} + \tfrac{1}{8}\, As_4 \uparrow \quad (38)$$

$$FeAs_{0.5} \xrightarrow{>1200^\circ C} \tfrac{1}{2}\, Fe_2As + \tfrac{1}{2}\, Fe \quad (39)$$

Thus, arsenic in the residues of thermal decomposition of arsenopyrite and iron arsenides at temperatures above 900-1200°C in inert atmosphere or vacuum can be present in the form of diiron arsenide [48,54,55].

4.2 Experimental

The resultant As-containing residue of DRM of Bakyrchik concentrate has been identified using EMPA, QEMSCAN, X-ray and neutron diffraction. Electron-microprobe analyses were performed on the iron-arsenic alloy using a Cameca SX 100 electron microprobe analyser. This operated at an excitation voltage of 25 keV, a specimen current of 20 nA, a peak-count time of 20 s, and a background-count time of 10 s. An ordinary thin section was prepared for microprobe analysis and embedded in epoxy resin. The sample was scanned using a 1 µm diameter beam spot and data were collected at 30 points for major phases and at least 5 points for minor phases at the surface. Six elements were analyzed using natural and synthetic standards. The following standards were employed: Cu, Sb, arsenopyrite, pyrite, and galena.

QEMSCAN analyses were performed by obtaining field-scans, that provided a characterisation of particle surfaces above a pre-defined electron backscatter threshold. The brightness coefficients were calibrated against quartz, gold and copper. Spectra were collected at 25 kV and 10 nA with 2000 total X-ray counts at a 5µg spacing, and compared to a Species Identification Protocol (SIP), which differentiate minerals using their characteristic X- ray and electron backscatter intensities. The iron-arsenic alloy sample was polished, mounted on resin and carbon coated (Figure 5). We extracted elemental maps of As, Fe, and Pb out of the QEMSCAN data.

Powder X-ray diffraction data were collected from randomly chosen portion of the iron-arsenic alloy to ensure that the sample mixing had been effective and that the sieving had not caused any phase segregation. The sample was ground into fine powder. In order to minimize preferred orientation the powder, with average particle size lower than 5 µm, was side loaded. The holder was a 2 mm thick flat Al holder. Measurements were collected at room temperature in the angular range 10-120° 2θ using a Bruker D8 Advance X-ray diffractometer operating with CuKα1(λ = 1.5406 Å) radiation. The powder patterns were refined by the Rietveld method with the GSAS-EXPGUI package [39,40] by using a pseudo-Voigt peak shape function [41] with the asymmetry correction [42]. The raw data were converted into GSAS file for EXPGUI using ConvX [43]. The crystallographic data used for the input are taken from ICSD website [44] and are given in supplementary materials. During the Rietveld refinement background coefficients, zero-shift error, cell parameters, peak shape parameters, preferred orientation with correction via the March-Dollase algorithm [45], and phase fractions were optimised.

Powder neutron diffraction data were recorded from the iron-arsenic alloy on the Fine Resolution Powder Diffractometer (FIREPOD) at the research reactor of the Helmholtz-Zentrum Berlin für Materialien

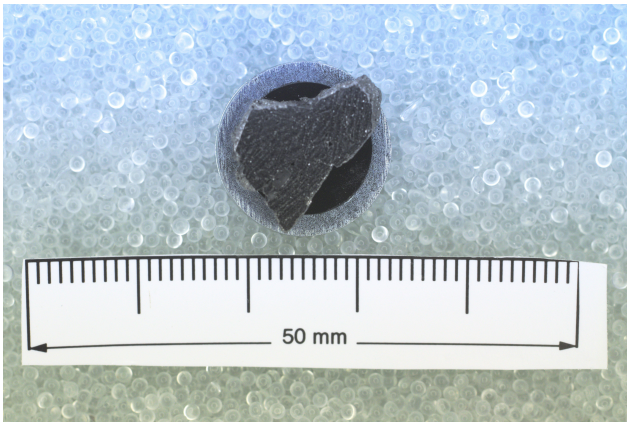

(a)

(b)

Figure 5: Photos of the iron-arsenic alloy, obtained by DRM of the Bakyrchik concentrate.

und Energie (HZB, Germany) [56]. The instrument is equipped with a Ge monochromator, providing an incident wavelength of 1.7982 Å. The powder was placed in a vanadium can. The sample diameter was 8 mm, and length about 40 mm. Data were collected at room temperature (294 K) in the range 3° - 142°, with binning size of 0.075° and refined with the Rietveld method using the software Topas V4.1 [57].

4.3 Results

Scanning electron microscope backscattered electron (BSE) images of the iron-arsenic alloy are presented in Figure 9. EPMA results showing representative compositions of major phases are given in Table 9.

In plane-polarized reflected light the iron-arsenic alloy appears grey with rare small reddish and white inclusions. The chemical compositions of phases were evaluated by energy dispersive spectroscopy (EDS). Close visual inspection of images demonstrates the presence of two major phases, consisting of Fe and As with minor to moderate substitution of Cu, Sb, S and Pb. The following minor phases were observed: AsS, FeS, Cu, Pb. It is likely that the white and reddish spots are AsS and Cu/FeS respectively. The primary major phase is grey, homogeneous and crystalline, whereas the secondary phase appears lighter and less

Table 9: Chemical analysis of major phases, wt. %

Amorphous phase						
Cu	Sb	As	S	Fe	Pb	Total
1.91	2.06	53.21	0.49	42.63	0.82	101.14
4.23	1.66	49.67	0.61	44.13	0.12	100.43
0.25	0.92	48.40	5.81	43.34	0.78	99.50
0	1.77	54.44	0.84	41.17	0.19	98.69
Crystalline phase						
Cu	Sb	As	S	Fe	Pb	Total
9.37	0	40.92	0.19	49.19	0	99.97
9.21	0	40.86	0.20	49.35	0	99.89
9.39	0	40.99	0.20	49.06	0	99.94
9.79	0	40.86	0.21	49.06	0	100.23

crystalline. Each phase was analysed at a minimum of 20 points.

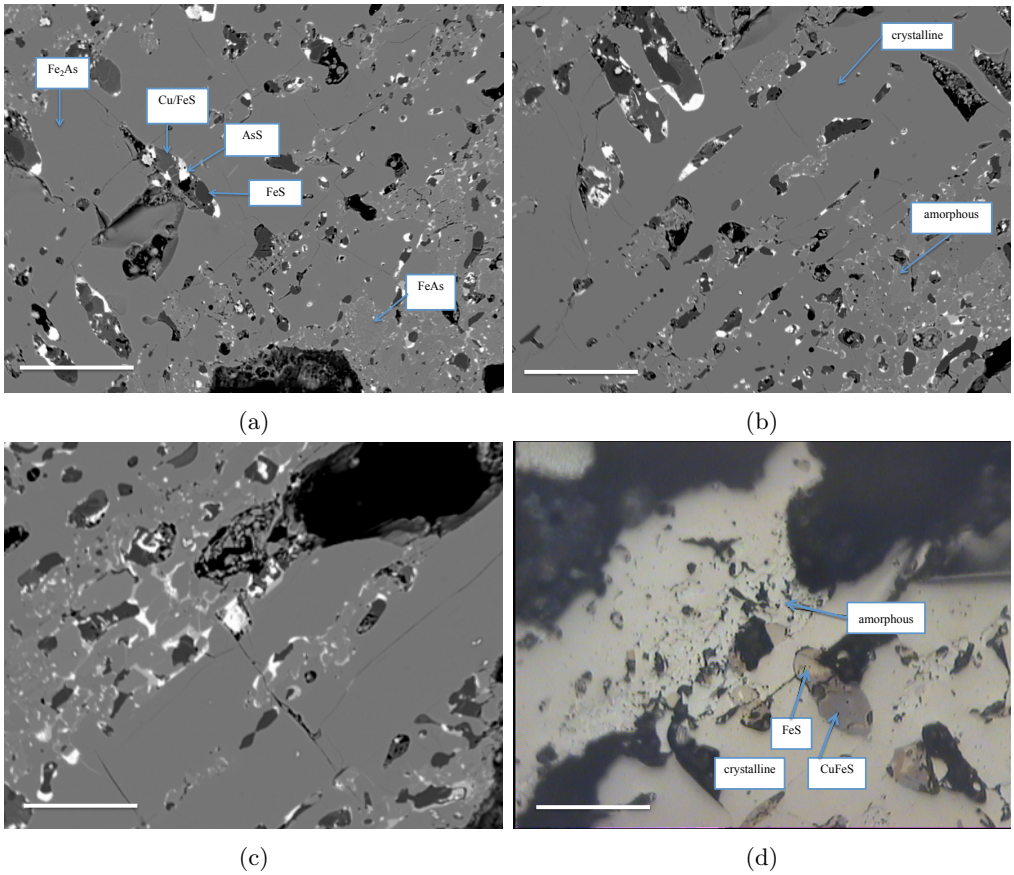

(a) (b)

(c) (d)

Figure 6: BSE (a-c) and optical image (d) of the iron-arsenic alloy. Scale bar 100 µm

Quantitative EPMA of iron-arsenic alloy. In order to quantify the phase composition of the iron-arsenic alloy the sample was scanned with a spot size of 1 micron and data were collected for major

phases at 30 points on the surface. Results of electron probe analysis has shown that the content of Fe_2As in the iron-arsenic alloy sample varies from 63.44 to 68.72%. The composition of the sample was calculated from the average of the data recorded at all points. Electron microprobe analysis shows that mean iron-arsenic alloy consists of 65.81% Fe_2As and 35.19% FeAs. However, in the vast majority of analyses the content of Fe_2As was about the modal value of 60-62% (Figure 7).

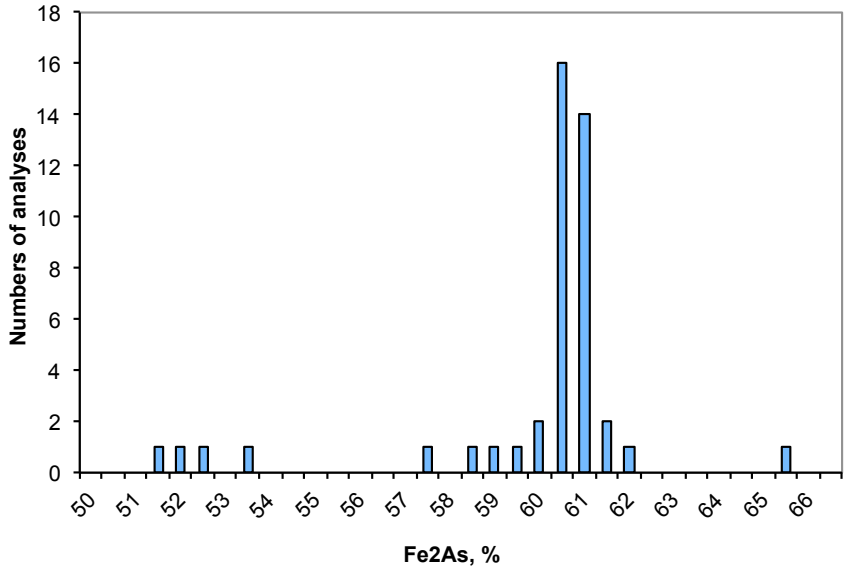

Figure 7: Proportion of Fe_2As in the major phases of iron-arsenic alloy

Elemental maps of As, Fe, and Pb are shown in Figure 8. In the arsenic map it is clearly shown that 58% of area is presented by phase containing 32-46% of As, which is close to composition of Fe_2As. 21% of area is occupied by the phase consisting of up to 32% arsenic. The rest 14% of area is represented by phases containing from 46 to 62% arsenic, which is close to composition of FeAs. Fe map shows the same pattern as on the As map, and confirms the composition of the alloy. Although As map is more accurate than Fe map in terms of area percent, probably, due to secondary fluorescence of Fe.

Rietveld refinement of the PXRD, and neutron powder diffraction patterns of the iron-arsenic alloy are plotted in Figures 9a and 9b. The neutron diffraction quantitative phase analysis of the iron-arsenic alloy in comparison with EMP and XRD analyses are given in Table 10.

The results of analyses slightly differ from each other. A possible explanation for this discrepancy might be that we used different specimens of the iron-arsenic alloy for each analyses. But the neutron results are more representative of the both, and XRD is skewed by sample absorption.

Quantitative phase analysis established that the iron-arsenic alloy comprises two major phases: Fe_2As and FeAs, with the former amounting to 65-67%. Small amount of lead (0.62%) has been detected in iron-arsenic alloy by PXRD analysis. Phase separation in the Pb-Fe-As system saturated with carbon at 1200°C was studied by Voisin et al., 2006 [65] in relation to the reductive smelting of lead sinter and scraps with high content of arsenic. They proposed a method to separate lead and arsenic to the corresponding alloys by smelting the initial lead-arsenic-containing material with iron in the presence of carbon at 1200°C. It

Table 10: Quantitative phase analyses of iron-arsenic alloy

Analysis	Identified phases					
	Fe_2As	FeAs	FeS	Pb	AsS	$FeSb_2$
EMP[a]	65.81	35.19	-	-	-	-
PXRD[c]	67.78	18.67	6.50	0.62	5.89	0.52
Neutron diffraction[b]	65.40	21.70	8.90	-	4.00	-

Note: [a]only major phases, [b]statistical indicators of the refinement: R_{wp}=11.73, χ^2=3.31, [c]statistical indicators of the refinement: R_{wp}=22, χ^2=18.7 .

has been found that mole fraction of iron in the lead-rich alloy phase as well as that of lead in iron-arsenic alloy was less than 0.003. In our study, DRM products were separated after cooling. We believe that lead content could be further minimised if DRM products would have been separated while they were liquid. Iron-arsenic alloy is dense, monolithic material, and does not require any solidification and/or stabilisation processes prior to disposal.

5 Conclusions

A feature of the Bakyrchik ores and concentrates is the microscopic inclusion of gold in the sulphide minerals and the presence of more than 10% of active carbon as well as arsenic, which complicates recovery during processing by conventional methods. An overview of the current state of investigations on the processing of refractory gold-arsenic bearing Bakyrchik concentrates demonstrated the need to develop new methods for processing refractory gold-arsenic bearing concentrates, allowing more efficient gold extraction and transforming arsenic into a low-toxic processing waste product, easy to store and dispose of.

A feasibility study of the DRM process for Bakyrchik concentrates has been carried out by conducting thermodynamic calculations. The thermodynamic calculations predicted the most probable interactions occurring during DRM of the gold-arsenic-bearing concentrates in reducing atmosphere and over a range of temperatures 1023-1523 K, and defined the expected mineralogy of the furnace charge, in which transformation of arsenic in a solid iron-arsenide-rich material and alloying of lead and gold into a metal phase are expected.

A systematic set of experiments has been used to determine optimal parameters for processing the DRM of Bakyrchik concentrates. This allowed us to obtain the optimal conditions of processing in the form of multifactorial equations related to the extraction of gold into crude lead, and arsenic into iron-arsenic alloy. The model provides the optimum technological parameters of the process, which allows extraction of 97% of gold into the lead bullion and conversion of 94-95% of arsenic into a convenient for disposal or transportation dense material.

Quantitative EMPA, X-ray and neutron diffraction analyses showed that iron-arsenic alloy consists of two major phases: Fe_2As and FeAs with the dominance of the former - about 65-67%. The Fe-As alloy is a compact monolithic, dense material, which could accommodate up to 40% arsenic. Furthermore, it doesn't require any troublesome and costly stabilisation/solidification pre-treatments prior to disposal. The result of the long-term leaching tests suggests that the iron-arsenic alloy, if disposed of in neutral to alkaline

conditions of monofills, would be a good medium for arsenic immobilisation. These advantages, together the high degree of gold extraction, make iron-arsenic alloy a very attractive waste form for removal of arsenic from refractory gold-arsenic-bearing concentrates.

In comparison to earlier methods used for gold recovery from the Bakyrchik concentrates, the approach presented here shows promising potential as an economically efficient and environmentally favourable method of gold recovery from double refractory carbonaceous gold-arsenic-bearing concentrates, and might be applicable both nationally and globally.

Acknowledgements

This work was supported by the Islamic Development Bank - Cambridge International Scholarship Programme. We express our sincere gratitude to BMV authorities for supply of the Bakychik concentrates. We also thank George Daher (SEE Geochem Manager, SGS Bulgaria) for the ICP-MS and fire assay analyses.

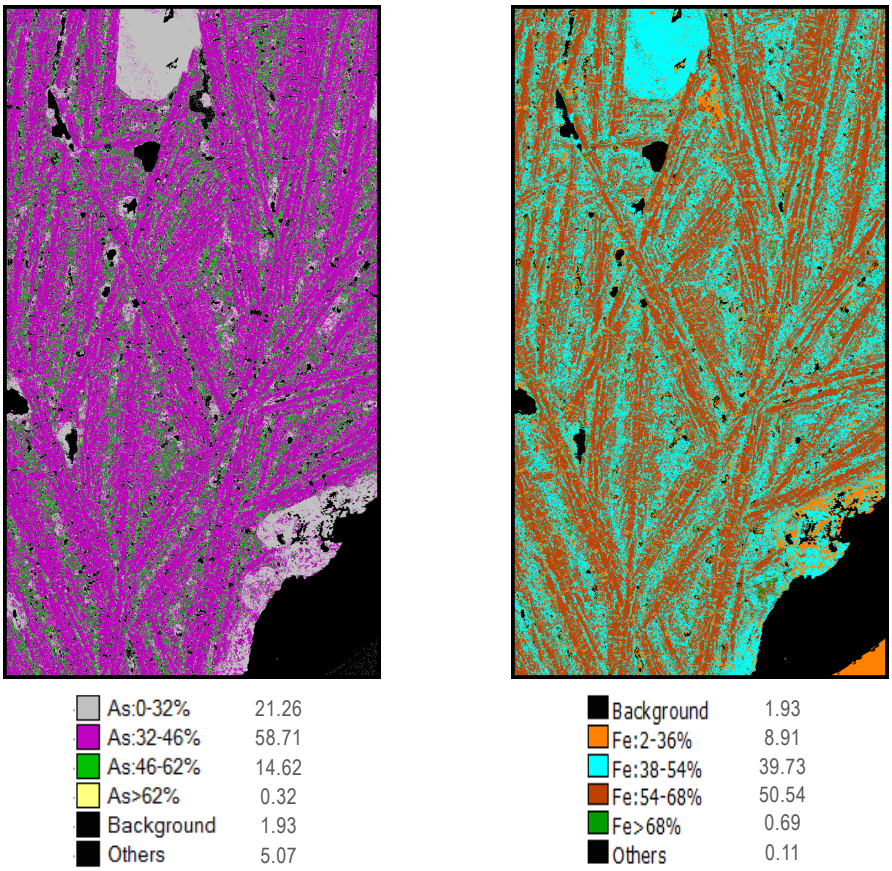

Figure 8: QEMSCAN elemental maps of the iron-arsenic alloy: (a) As, (b) Fe, and (c) Pb

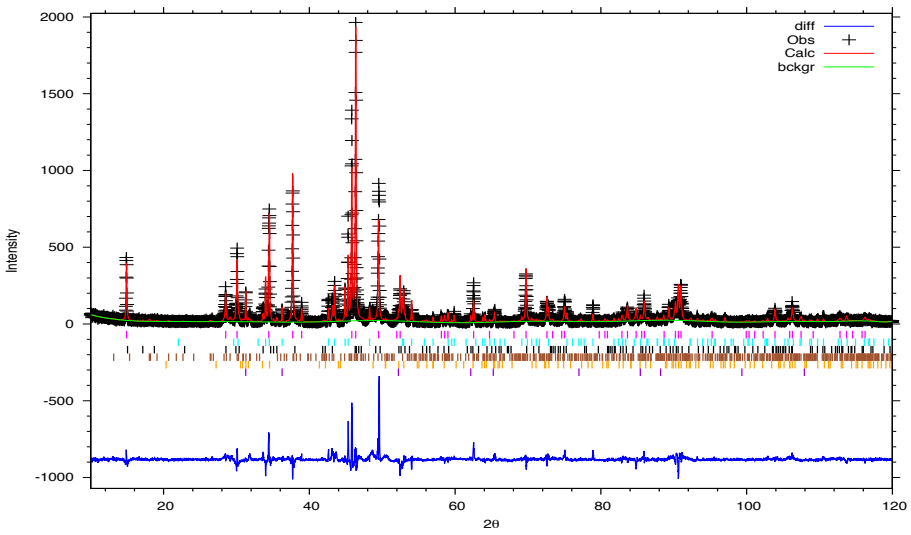

(a)

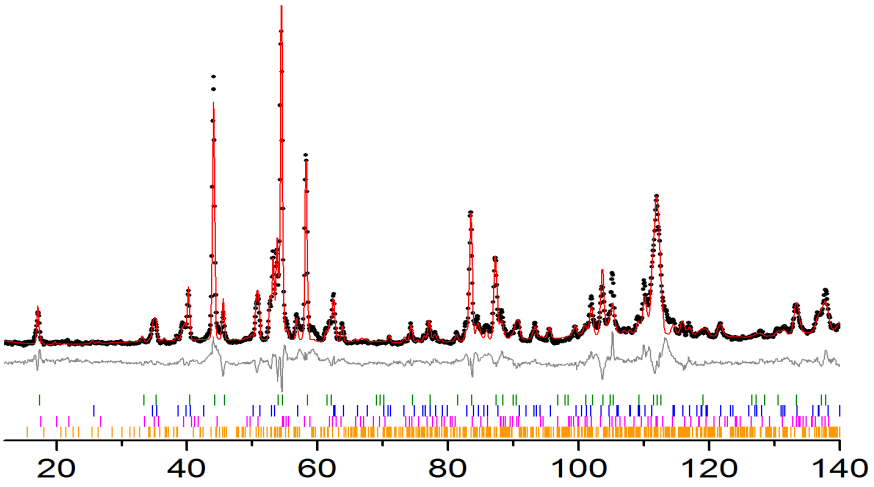

(b)

Figure 9: Rietveld refinement of the (a) PXRD data of the iron-arsenic alloy. The tick marks are identified phases: Fe_2As, FeAs, FeS, AsS, $FeSb_2$, Pb (from top to bottom), and (b) Rietveld refinement of the neutron powder diffraction pattern. X axis is in degrees of 2θ. The tickmarks are identified phases: Fe_2As, FeAs, FeS, AsS (from top to bottom)

References

[1] SR La Brooy, HG Linge, and GS Walker. Review of gold extraction from ores. *Minerals Engineering*, 7(10):1213–1241, 1994.

[2] JP Vaughan. The process mineralogy of gold: The classification of ore types. *Journal of the Minerals Metals and Materials Society*, 56(7):46–48, 2004.

[3] PM Afenya. Treatment of carbonaceous refractory gold ores. *Minerals Engineering*, 4(7-11):1043–1055, 1991. ISSN 0892-6875.

[4] ID Fridman, EE Savari, NN Demina, NP Silina, and PV Inshin. Study of the sorption properties of native carbonaceous substances in the cyaniding process. *Journal of applied chemistry (USSR)*, 53(9): 1453–1457, 1980. ISSN 0021-888X.

[5] VV Lodeischikov. *Technology to recover gold and silver from refractory ores*. Irgiredmet JSC. Irkutsk, 1999.

[6] DM Hausen. Processing Gold Quarry refractory ores. *Journal of the Minerals Metals and Materials Society*, 41(4):43–45, 1989.

[7] WJ Guay and MA Gross. The treatment of refractory gold ores containing carbonaceous material and sulfides. *Society of Mining Engineers of AIME*, (81-45):1–4, 1981.

[8] K Osseo-Asare, PM Afenya, and GMK Abotsi. Carbonaceous matter in gold ores: isolation, characterization and adsorption behavior in aurocyanide solutions. In *Precious metals: Mining, extraction and processing*, pages 125–144, Los-Angeles, 1984.

[9] IA Zhuchkov. Opyt pererabotki upornykh zolotosoderzhashchikh rud (in rus). *Tsvetnaya metallurgiya*, (10):22–24, 1970.

[10] RW Nice. Recovery of gold from active carbonaceous ores at McIntyre. *Canadian Mining Journal*, 92 (6):41, 1971.

[11] AS Radtke and BJ Scheiner. Studies of hydrothermal gold deposition (pt.1), Carlin gold deposit, Nevada, the role of carbonaceous materials in gold deposition. *Economic Geology*, 65(2):87–102, 1970.

[12] ES Leaver and JA Woolf. Re-treatment of Mother Lode (California) carbonaceous slime tailings. Tech. Paper, US Bureau of Mines, 1930.

[13] RJ Adamson. *Gold Metallurgy in South Africa*. Chamber of Mines of South Africa, Johannesburg, South Africa, 1972.

[14] Official site of the President of the Republic of Kazakhstan (2016), The Republic of Kazakhstan. URL `http://www.akorda.kz/`. Available from: http://www.akorda.kz/. Accessed 25 February 2016.

[15] Polymetal International Plc (2016), Kyzyl Project. URL `http://www.polymetalinternational.com/`. Available from: http://www.polymetalinternational.com/. Accessed 25 February 2016.

[16] Turquoise Hill Resources (2016), Altynalmas Gold's new upgraded and confirmed Bakyrchik East Mineral Resource Gold deposit boosts total gold resources at Kyzyl Project in Kazakhstan. URL `http://www.turquoisehill.com`. Available from: http://www.turquoisehill.com/i/pdf/NR-Aug-3-11-2-all.pdf. Accessed 1 January 2016.

[17] PI Poltorikhin. Gold contents of pyrites in the Kalba gold belt. *International Geology Review*, 16(2): 154–155, 1974.

[18] VA Narseev, UV Gostev, AV Zakharov, DM Kozlyaninov, VN Matvienko, VA Favorov, NM Frankovskaya, and AA Shiganov. *The Bakyrchik Deposit (Geology, Geochemistry, Mineralization)*. Moscow, TsNIGRI, 2001.

[19] G Levitan. *Gold Deposits of the CIS*. Xlibris: Philadelphia, 2008.

[20] KE Haque. Gold leaching from refractory ores-literature survey. *Mineral Processing and Extractive Metallurgy Review*, 2(3):235–253, 1987. doi: 10.1080/08827508708952607. URL `http://dx.doi.org/10.1080/08827508708952607`.

[21] A Wusaty and D Douglas. Bakyrchik mining venture. Kyzyl Gold Project. Environmental Feasibility Study, Sustainability Pty Ltd., 2011.

[22] Kyzyl Gold Project. Technical report, Roscoe Postle Associates, 2010.

[23] L Kushakova and A Muszer. Optimisation of roasting of arsenic-carbon refractory gold ores for cyanide leaching. *Physicochemical Problems of Mineral Processing*, (43):59–64, 2009.

[24] NA Kolesnikov, VI Kazakov, and II Bahtina. Dvuhstadialnyi obzhig v kipyashem sloe upornyh zolotomyshyakovyh kontsentratov (in rus). *Izvestiya VUZov: Tsvetnaya metallurgiya*, (3):21–26, 1986.

[25] IA Zhuchkov and VV Lodeischikov. K voprosu izvlechenia zolota iz upornyh sulfidnyh kontsentratov s tonkovkraplennym zolotom (in rus). In *Trudy Irgiredmeta*, 1972.

[26] KE Sobel, L Bolinski, and KA Foo. Pilot-plant evaluation of the Redox process for Bakyrchik Gold Plc. *Minerals Engineering*, 8(4-5):431–440, 1995.

[27] AR Kosmuhambetov. Nauchnye osnovy oksigidrohlorinatsionnyh, elektromembrannyh protsessov i primenenie v gidrometallurgii tsvetnyh, redkih i blagorodnyh metallov: avtoref. dok. tehn. nauk (in rus). Almaty, 2006.

[28] EN Sazhin, VA Luganov, and GA Plahin. Vyvod myshyaka pri pererabotke vysokomyshiakovistyh mednyh kontsentratov (in rus). *Kompleksnoe ispolzovanie mineralnogo syria*, (4):50–51, 1987.

[29] SM Isabaev and H Kuzgibekova. Tehnologicheskaya shema pererabotki zolotosoderzhashih kontsentratov (in rus). *Promyshlennost' Kazahstana*, (1):76–77, 2000.

[30] VE Khrapunov and RA Isakova. *Pererabotka upornyh zolotomyshiakovyh kontsentratov s primeneniem vakuuma (in rus)*. Almaty: NITS Gylym, 2002.

[31] LS Chelohsaev, RA Isakova, BZ Tarasenko, et al. Opytno-promyshlennye ispytaniya vakuumtermicheskogo vydeleniya myshyaka iz zolotosoderzhashih flotatsionnyh kontsentratov (in rus). *Tsvetnye metally*, (9):25–27, 1980.

[32] AU Shustrov, UA Matsenko, and VI Maslov. Razrabotka tehnologii pererabotki flotatsionnogo zolotogo kontsentrata metodom sodovoi plavki (in rus). *Tsvetnye metally*, (10):29–31, 1999.

[33] N Chakraborti and DC Lynch. Thermodynamics of roasting arsenopyrite. *Metallurgical Transactions B*, 14(2):239–251, 1983. ISSN 0360-2141.

[34] Mark G Aylmore and Frank J Lincoln. Mechanochemical milling-induced reactions between gases and sulfide minerals: Ii. reactions of co 2 with arsenopyrite, pyrrhotite and pyrite. *Journal of alloys and compounds*, 314(1):103–113, 2001.

[35] A Seitkan and S A T Redfern. KZ Patent N 2015/0394.1 Method of processing gold-arsenic-bearing sulfide concentrates (in rus), March 2016. URL `http://www.kazpatent.kz/images/bulleten/2016/`.

[36] VA Ryabin, MA Ostroumov, and TF Svit. *Termodinamicheskie svoistva veshestv. Spravochnik (in rus)*. L.:Himia, 1977.

[37] Outotec (2016), Chemical reaction and equilibrium software HSC Chemistry. URL `http://www.outotec.com`. Available from: http://www.outotec.com/en/Products–services/HSC-Chemistry/. Accessed 16 February 2016.

[38] H Rau. Vapour composition and van der Waals constants of arsenic. *The Journal of Chemical Thermodynamics*, 7(1):27 – 32, 1975. ISSN 0021-9614. doi: http://dx.doi.org/10.1016/0021-9614(75)90077-4. URL `http://www.sciencedirect.com/science/article/pii/0021961475900774`.

[39] AC Larsen and RB Von Dreele. GSAS, General Structure Analysis System. *LANSCE, MS-H805, Los Alamos National Laboratory, Los Alamos, New Mexico*, 1994.

[40] BH Toby. EXPGUI, a graphical user interface for GSAS. *Journal of applied crystallography*, 34(2): 210–213, 2001.

[41] P Thompson, DE Cox, and JB Hastings. Rietveld refinement of Debye-Scherrer synchrotron X-ray data from Al_2O_3. *Journal of Applied Crystallography*, 20(2):79–83, 1987.

[42] LW Finger, DE Cox, and AP Jephcoat. A correction for powder diffraction peak asymmetry due to axial divergence. *Journal of Applied Crystallography*, 27(6):892–900, 1994.

[43] M Bowden. ConvX (2015). URL `http://www.ccp14.ac.uk/ccp/web-mirrors/convx/`. Available from: http://www.ccp14.ac.uk/ccp/web-mirrors/convx/. Accessed 25 February 2016.

[44] Inorganic Crystal Structure Database (2015). URL `http://icsd.cds.rsc.org/search/basic.xhtml`. Available from: http://icsd.cds.rsc.org/search/basic.xhtml. Accessed 15 September 2015.

[45] WA Dollase. Correction of intensities for preferred orientation in powder diffractometry: application of the March model. *Journal of Applied Crystallography*, 19(4):267–272, 1986.

[46] MM Protodyakonov and RI Teder. *Metodika ratsionalnogo planirovaniya eksperimenta (in rus)*. Moscow, Nauka, 1970.

[47] VP Malyhsev. *Veroyatnostno-determinirovannoe planirovanie eksperimenta (in rus)*. Alma-Ata, Nauka, 1981.

[48] VE Khrapunov, RA Isakova, MM Spivak, and IO Fedulov. Dissotsiatsia diarsenida zheleza (in rus). *Zhurnal neorganicheskoi khimii*, 38(5):784–785, 1993.

[49] PB Barton. Thermochemical study of the system Fe-As-S. *Geochimica et Cosmochimica Acta*, 33(7): 841–857, 1969.

[50] BA Strathdee and LM Pidgeon. Thermal decomposition and vapor pressure measurements of arsenopyrite and arsenical ore. *Canadian Mining and Metallurgical Bulletin*, 54(596):883 – 887, 1961.

[51] IA Zhuchkov and VN Smagunov. O mekhanizme okisleniya arsenopirita (in rus). *Prikladnaya khimiya*, 44(8):1680–1688, 1971.

[52] SM Isabayev, AS Pashinkin, EG Mil'ke, and MI Zhambekov. *Fiziko-khimicheskiye osnovy sul'fidirovaniya mysh'yaksoderzhashchikh soyedineniy (in rus)*. Alma-Ata: Nauka, 1986.

[53] EN Shlyapkina. Termograficheskie harakteristiki sulfidnyh mineralov: avtoref. kand. tehn. nauk (in rus). Kazan, 1972.

[54] VE Khrapunov, MM Spivak, VA Spitsyn, AS Khlystov, RA Isakova, and IO Fedulov. O termicheskom povedenii arsenopirita (in rus). *Zhurnal neorganicheskoi khimii*, 36(11):2786 – 2790, 1991.

[55] MA Tkach, OB Tkachenko, and LE Isakova, RA Ugryumova. O povedenii arsenidov zheleza pri nagrevanii v vakuume (in rus). In *Trudy IMiO AN Kaz. SSR*, volume 52, pages 54–60, 1977.

[56] DM Többens, N Stüßer, K Knorr, HM Mayer, and G Lampert. E9: the new high-resolution neutron powder diffractometer at the Berlin neutron scattering center. In *Materials Science Forum*, volume 378, pages 288–293. Trans Tech Publ, 2001.

[57] A Coelho. TOPAS-Academic. Coelho Software, Brisbane, Australia, 2007.

[58] H Okamoto. The As-Fe (arsenic-iron) system. *Journal of phase equilibria*, 12(4):457–461, 1991.

[59] D Schiferl and CS Barrett. The crystal structure of arsenic at 4.2, 78 and 299 k. *Journal of Applied Crystallography*, 2(1):30–36, 1969.

[60] P Ondrus, I Vavrin, R Skala, and F Veselovsky. Low-temperature ni-rich lollingite from haje, pribram, czech republic. rietveld crystal structure refinement. *Neues Jahrbuch fur Mineralogie-Monatshefte*, (4): 169–185, 2001.

[61] K Selte and A Kjekshus. The crystal structure of FeAs. *Acta Chemica Scandinavica*, 23:2047 —2054, 1969.

[62] J Nuss, U Wedig, and M Jansen. Geometric variations and electron localizations in intermetallics: PbFCl type compounds. *Zeitschrift für Kristallographie-Crystalline Materials*, 221(5-7):554–562, 2006.

[63] R Kohlhaas. Magnetische und kalorimetrische studien an eisen, kobalt und nickel in bereich höher temperaturen: Hochtemperaturverhalten magnetischer werkstoffe. In *Magnetismus: Struktur und Eigenschaften Magnetischer Festkorper*, pages 134–159. VEB Deutscher Verlag für Grundstoffindustrie Leipzig, 1967.

[64] ME Straumanis and DC Kim. Lattice constants, thermal expansion coefficients, densities, and perfection of structure of pure iron and of iron loaded with hydrogen. *Z METALLKUNDE*, 60(4):272–277, 1969.

[65] Leandro Voisin, Hector M Henao, Mitsuhisa Hino, and Kimio Itagaki. Phase relations, activities and minor elements distribution in fe-pb-as and fe-pb-sb systems saturated with carbon at 1473 k. *Materials transactions*, 46(12):3030–3036, 2005.

[66] VA Muratova. Fiziko-himicheskie svoistva arsenopirita i arsenidov zheleza: avtoref. kand. tehn. nauk (in rus). Moscow, 1989.

[67] GV Naumov, BN Ryzhenko, and IA Hodakovskii. *Spravochnik termodinamicheskih velichin (in rus)*. Moscow, Atomizdat, 1971.

[68] HT Evans. Lunar troilite: crystallography. *Science*, 167(3918):621–623, 1970.

[69] F Pertlik. Kristallstrukturbestimmung der monoklinen hochtemperaturmodifikation von AsS (-AsS). *Österreichische Akad. Wissenschaften (Austrian Acad. Sci.) Math.-Natur. Sitzungsberichte*, 131:3–5, 1994.

[70] N Bouad, L Chapon, R-M Marin-Ayral, F Bouree-Vigneron, and J-C Tedenac. Neutron powder diffraction study of strain and crystallite size in mechanically alloyed PbTe. *Journal of Solid State Chemistry*, 173(1):189–195, 2003.

[71] RL Blake, RE Hessevic, T Zoltai, and LW Finger. Refinement of hematite structure. *American Mineralogist*, 51(1-2):123, 1966.

[72] H Fjellvåg, F Grønvold, S Stølen, and B Hauback. On the crystallographic and magnetic structures of nearly stoichiometric iron monoxide. *Journal of Solid State Chemistry*, 124(1):52–57, 1996.

[73] H Fuess, T Kratz, J Töpel-Schadt, and G Miehe. Crystal structure refinement and electron microscopy of arsenopyrite. *Zeitschrift für Kristallographie-Crystalline Materials*, 179(1-4):335–346, 1987.

[74] W Paszkowicz and JA Leiro. Rietveld refinement study of pyrite crystals. *Journal of alloys and compounds*, 401(1):289–295, 2005.

[75] A Amisano-Canesi, G Chiari, G Ferraris, G Ivaldi, and S Soboleva. Muscovite-and phengite-3T: crystal structure and conditions of formation. *European Journal of Mineralogy*, 6(4):489–496, 1994.

[76] P Trucano and R Chen. Structure of graphite by neutron diffraction. *Nature*, 258:136–137, 1975.

[77] K Tomita, K Shiraki, and M Kawano. Crystal structure of dehydroxylated 2M1 sericite and its relationship with mixed-layer mica/smectite. *Clay Science*, 10(5):423–441, 1998.

[78] K Kihara. An X-ray study of the temperature dependence of the quartz structure. *European Journal of Mineralogy*, (2):63–78, 1990.

[79] Y Ohashi and LW Finger. Stepwise cation ordering in bustamite and disordering in wollastonite. *Carnegie Inst Washington Yearb*, 75:746–754, 1976.

Supplementary material

Table 11: Reference thermodynamic characteristics of the reactants relevant to the furnace charge

Phase	ΔH^0_{298}	S^0_{298}	$C_{P_{298}}$	$C_p = a + bT + cT^{-2}$, J/(mol K)			T, K
				a	$b \times 10^{-3}$	$c \times 10^5$	
As_4 (g)	143.68	329.70	77.40	83.07	-	-5.02	298-2000
As_2 (g)	193.80	242.37	35.13	37.39	-	-2.18	298-2000
As_4S_4 (g)	-5.44	451.45	164.01	177.44	7.95	-13.81	298-1073
As_2O_3 (g)	-656.89	107.11		35.04	203.5	-	273-548
FeAsS* (s)	-137.03	67.95	68.49	62.88	40.55	-1.42	298-975
FeS (s)	-100.42	60.29	50.54	51.04	9.95	-	598-1468
FeS_2 (s)	-163.18	53.05	62.17	74.81	5.52	-12.76	298-1100
S_2 (g)	127.52	228.04	35.73	36.48	0.67	-3.77	298-3000
Fe (s)	0	27.15	24.98	17.50	24.79	-	273-1033
$FeAs_2$* (s)	-85.73	80.21	70.88	76.15	3.92	3.97	298-1173
Fe_2As** (s)	-4.60	144.64	72.93	76.74	0.48	3.92	298-1173
FeAs* (s)	-43.47	60.00	50.58	35.32	44.06	7.14	298-1173
FeO(s)	-265.0	60.79	49.95	51.83	6.78	-1.59	298-1200
PbO (s)	-219.43	66,20	45.80	37.89	26.79	-	298-1000
Pb (s)	0	64.85	26.46	23.57	9.76	-	273-600
C (s)	0	5.74	8.54	17.17	4.27	-8.79	298-2300
CO (g)	-110.60	197.68	29.132	28.43	4.10	-0.46	298-2500
CO_2 (g)	-393.77	213.82	37.14	44.17	9.04	-8.54	298-2500
SO_2 (g)	-296.90	248.07	39.87	46.19	7.87	-7.7	298-2000

All from [36], * - from [66], ** - from [67]

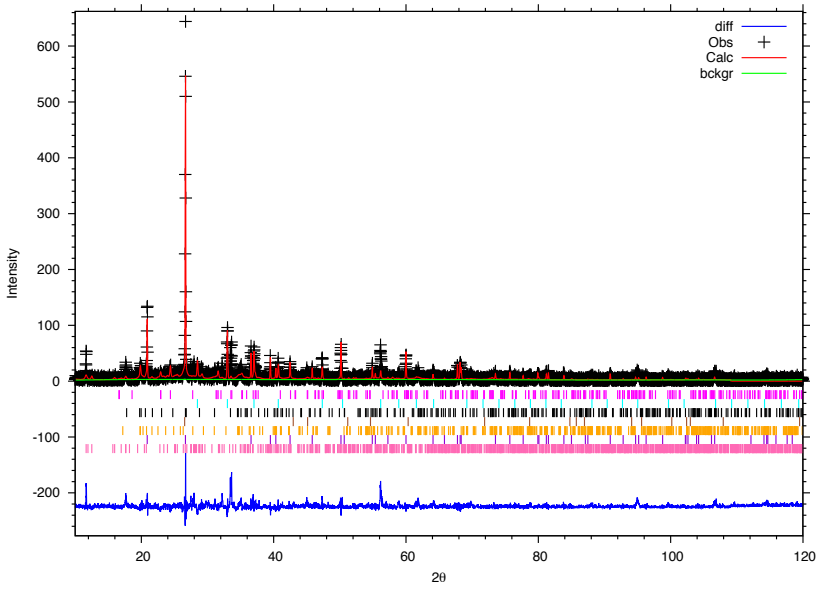

BC1

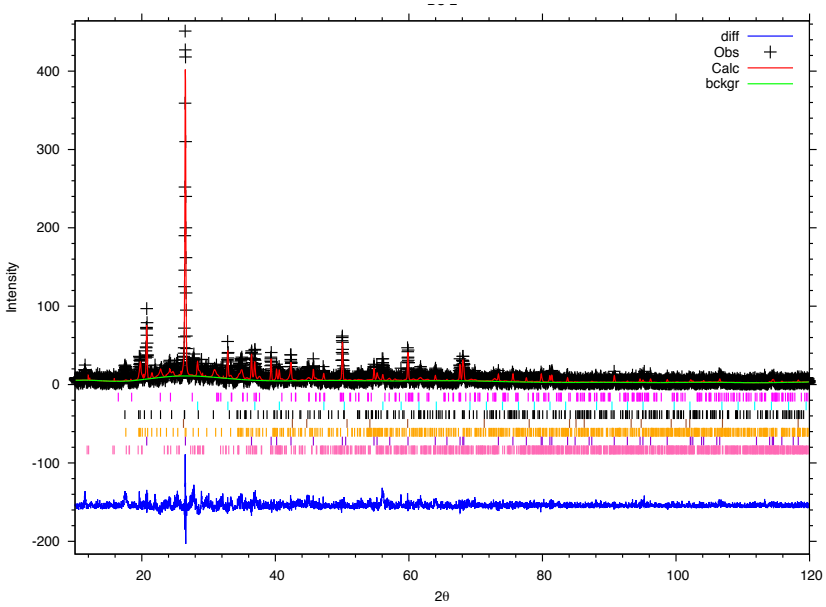

BC2

Figure 10: Rietveld refinements of the PXRD patterns of the Bakyrchik concentrate samples. The tick marks are positions of reflections in the phases fitted: arsenopyrite, pyrite, muscovite, graphite, sericite, quartz, wollastonite (from top to bottom).

Table 12: Crystallographic data

Phase	Chemical formula	Space group	ICSD collection code	Reference
Iron arsenide (2/1)	Fe_2As	P4/n m m	415628	[62]
Iron (III) arsenide	FeAs	P n a 21	15009	[61]
Iron sulfide	FeS	P-6 2 c	31963	[68]
Arsenic sulfide	AsS	C 1 2/c 1	86628	[69]
Lead	Pb	F m -3 m	46501	[70]
Iron (III) oxide	Fe_2O_3	R -3 c H	15840	[71]
Iron (II) oxide	FeO	F m -3 m	82233	[72]
Arsenopyrite	FeAsS	C 1 1 21/d	62400	[73]
Pyrite	FeS_2	P a -3	152784	[74]
Muscovite		P 31 1 2	75952	[75]
Graphite		P 63/m m c	76767	[76]
Sericite		C 1 2/c 1	87447	[77]
Quartz		P 32 2 1	89276	[78]
Wollastonite		C -1	34168	[79]